



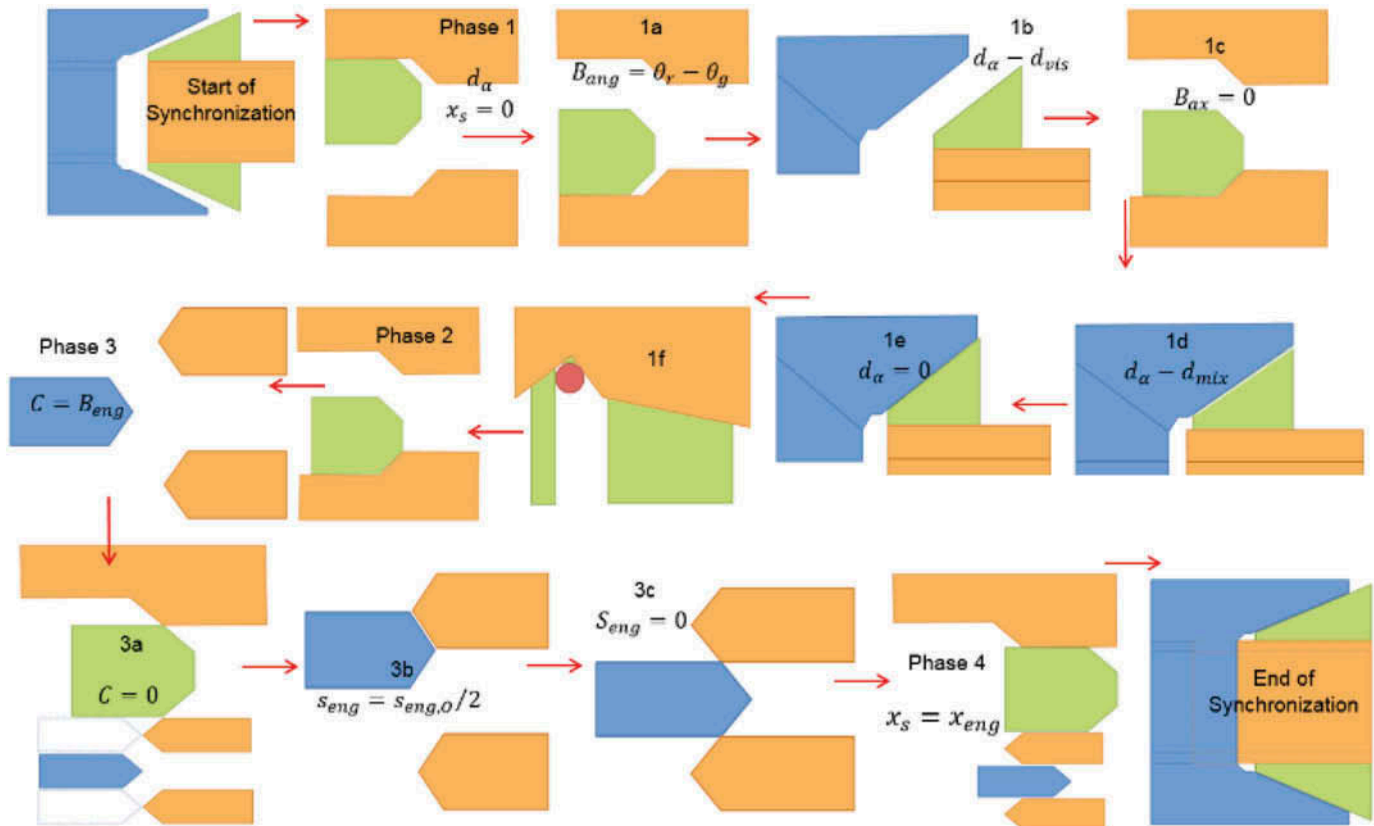
Performance improvement of a transmission synchronizer via sensitivity analysis and Pareto optimization

Downloaded from: <https://research.chalmers.se>, 2025-12-04 10:16 UTC

Citation for the original published paper (version of record):

Irfan, M., Berbyuk, V., Johansson, H. (2018). Performance improvement of a transmission synchronizer via sensitivity analysis and Pareto optimization. *Cogent Engineering*, 5(1): 1-46. <http://dx.doi.org/10.1080/23311916.2018.1471768>

N.B. When citing this work, cite the original published paper.



MECHANICAL ENGINEERING | RESEARCH ARTICLE

Performance improvement of a transmission synchronizer via sensitivity analysis and Pareto optimization

Muhammad Irfan, Viktor Berbyuk and Håkan Johansson

Cogent Engineering (2018), 5: 1471768



Received 10 August 2016
Accepted 13 February 2017
First Published 21 May 2018

*Corresponding author: Muhammad Irfan, Division of Dynamics, Department of Mechanics and Maritime Sciences, Chalmers University of Technology, SE-412 96 Gothenburg, Sweden
E-mail: irfan.muhammad@chalmers.se

Reviewing Editor:
Duc Pham, University of Birmingham, United Kingdom

Additional information is available at the end of the article

MECHANICAL ENGINEERING | RESEARCH ARTICLE

Performance improvement of a transmission synchronizer via sensitivity analysis and Pareto optimization

Muhammad Irfan^{1*}, Viktor Berbyuk¹ and Håkan Johansson¹

Abstract: Gear-shifting mechanism has a key role in transmission system of a vehicle. During gear shifting, there is a risk of losing the engine optimal speed that will ultimately lead to more emission from the vehicle. It is demanded for optimal performance of transmission systems to increase quality of synchronizer used for gear shifting. Especially in the case of heavy vehicles, the synchronizer performance needs to be robust more even during different operating scenarios. Synchronization process varies by changing its parameters values. So one of the ways to improve performance of the synchronizer is to optimizing its parameters. In the paper, a generic synchronizer mechanism (GSM) is considered. Mathematical model of GSM is presented based on constrained Lagrangian formalism (CLF) and detailed kinematics of synchronization process in transmission system. Speed difference at the end of the main synchronization phase and synchronization time are chosen as two objectives. The following eight parameters of the synchronizer have taken as input parameters: cone angle, cone coefficient of friction, cone radius, rate of shift force, blocker angle, blocker coefficient of friction, gear moment of inertia, and ring moment of inertia. Influence of the parameters on objectives is studied. The values of the objective functions decrease with increasing some of the parameters and increase with increasing others. Not only the

ABOUT THE AUTHORS

PhD student Muhammad Irfan, Professor Viktor Berbyuk and associate professor Håkan Johansson are employed at the division of Dynamics, Department of Mechanics and Maritime Sciences at Chalmers University of Technology, Gothenburg, Sweden. The present work is a part of the research of transmission cluster with collaboration of AB Volvo, Scania CV AB, Royal Institute of Technology, Chalmers University of Technology and the Swedish Agency for Innovation Systems (VINNOVA). Main objectives of the project are to increase service life of the synchronizer without compromising the shift quality and its properties, minimize the performance variations over the service life, and to develop a computer based tool to evaluate the new conceptual design.

PUBLIC INTEREST STATEMENT

The aim of this work is to meet the need of future to increase overall efficiency by reducing fuel consumption for internal combustion engine. The engine needs to operate in favorable conditions with respect to torque and speed. Shifting of the gear should be faster and frequent. This leads to increased strain on the gearbox and further on gear-shifting mechanism. Existing engineering tools still need improvements to analyze the gear-shifting processes. The overall objective of the project is to develop new knowledge and optimize gear-shifting mechanism regarding service life, energy consumption, switching quality, and robustness. Therefore, a mathematical model of a generalized gear-shifting mechanism is developed and analyzed by sensitivity analysis. The model represents complete gear-shifting process and is flexible to adapt to different synchronizer designs. The multi-objective optimization problem of choosing structural parameters to obtain quick and smooth gear shifting is studied.

objective functions have opposite behavior between the parameters but also have opposite behavior with variation of the same parameters. For example, the synchronization time decreases but the speed difference increases with increasing cone coefficient of friction. The Matlab routine of multi-objective optimization is applied to obtain the optimized parameter values of the generic synchronizer at different operating conditions. In the first case, the sleeve is considered as a master, in the second case the gear is considered as master, and in the third case both sleeve and gear are considered as slaves. In each case, three different operating conditions are studied which are nominal, transmission vibrations, and road grade. The obtained results of biobjective optimization (Pareto fronts, Pareto sets, and corresponding performance diagrams) are analyzed and the most influencing synchronizer parameters have been identified.

Subjects: Dynamics and Kinematics; General Systems; Automotive Technology and Engineering

Keywords: generic synchronizer; quickness; smoothness; Pareto optimization; road grade; vibrations

1. Introduction

The synchronizer is a mechanism that is commonly used in heavy vehicles' transmissions to ensure quick and smooth gear shifting. New engine designs developed to meet demands for higher power output and reduced fuel consumptions require more frequent gear shifting under higher loads. To this end, enhancing the performance of the synchronizer mechanism is crucial and is, therefore, receiving increasing attention in the engineering community as well as academia (Abel, Schreiber, & Schindler, 2006; Berbyuk, 2015; Gong, Zhang, Chen, & Wang, 2008; Gustavsson, 2009; Häggström, Sellgren, Stenström, & Björklund, 2015; Häggström, 2016; Häggström & Nordlander, 2011; Häggström, Nyman, Sellgren, & Björklund, 2016; Hoshino, 1999; Irfan, Berbyuk and Johansson, 2015a, 2015b; Irfan, Berbyuk, & Johansson, 2016; Kelly & Kent, 2000; Liu & Tseng, 2007; Lovas, 2004; Razzacki & Hottenstein, 2007; Sahlholm & Johansson, 2010; Sandooja, 2012; Sharma & Salva, 2012; Stenvall, 2010; Yuming, 2011).

Lovas (2004), for instance, highlighted the importance of synchronizer behavior by pointing out the problems of stick-slip, double bump, etc., incorporated mathematical models in a numerical simulation software, confronted simulation results with test bench results, and gave some suggestion to improve the synchronizer performance. Abel et al. (2006) addressed comfort optimization challenges of the dual-clutch transmission system and illustrated modeling solutions. Gong et al. (2008) analyzed synchronization theoretically and with shift robot. Gustavsson (2009) focused on control design to obtain a smooth movement of the synchronizer sleeve. A simulation technique developed to clarify abnormality of the shift force in Hoshino (1999; Liu & Tseng, 2007). Häggström and Nordlander (2011) developed user-friendly Matlab program for synchronization. (Kelly and Kent (2000) presented a dynamic model to highlight the gear-shifting problems. Razzacki and Hottenstein (2007) established a mathematical relationship between the synchronizer parameters and verified those experimentally. Sandooja (2012) provided simulation of higher level of gear-shifting performance and analytical results. Sharma and Salva (2012) dealt with techniques to reduce the double bump. Yuming (2011) introduced working principle, listed the designing formula and parameters and designing principle. Irfan, Berbyuk and Johansson (2015a, 2015b; Irfan et al., 2016) have developed a mathematical model of the generic synchronizer with five degrees of freedom based on constrained Lagrangian formalism (CLF) and studied sensitivity of the synchronization time and speed difference with respect to three synchronizer parameters and optimize the synchronization. The development of two types of numerical models for the synchronization process, namely fluid-structure interaction to simulate the presynchronization phase and

thermomechanical FE models to simulate the main synchronization phase, are presented by Haggström (2016).

However, these studies do not address the design problem of finding the most suitable set of structural parameters to optimize the synchronization process. Main focus of the study is to optimize the synchronization process and highlight the most influencing parameters of the synchronizer performance. The generic synchronizer presented in Irfan, Berbyuk and Johansson (2015a) has been used for analysis. Performance of synchronization process is measured by noticing the time for complete gear shifting and the speed difference at end of the main synchronization. Sensitivity of the parameters is studied based on two performance measures; synchronization time and speed difference. The mathematical statement of the biobjective Pareto optimization problem is given and Matlab routine of multi-objective optimization is used to obtain Pareto front between the synchronization time and the speed difference. The values of eight parameters from Pareto set analyzed with Pareto front to find out the trends. The most influencing parameters found by looking at the trends of parameters, percentage change of their values within the optimized range, and trends of the objectives with increasing parameters. Three scenarios under three cases are studied. The three scenarios are nominal case, road grade and transmission vibrations. The three cases are sleeve as a master, gear as a master and both sleeve and gear as slaves. The most influencing parameters in each scenario at every case are presented at the end.

2. A generic synchronizer and synchronization

A generic synchronizer introduced in Irfan, Berbyuk and Johansson (2015a) is considered for sensitivity analysis and optimization. The generic synchronizer as shown in Figure 1 consists of three main bodies: engaging sleeve, synchronizer ring, and gearwheel. The sleeve has engaging teeth and a frictional cone, the ring has a frictional cone and blocker and the gearwheel has blocker and engaging teeth. The synchronization process is the process of engaging the sleeve and gearwheel teeth after reducing the speed difference between the engaging bodies. To reduce the speed difference frictional cones slide over each other. A blocker contact is used to stop the axial movement of the sleeve from going further for teeth engagement until the speed difference reduces to a certain level.

A multibody system modeled the generic synchronizer has five degrees of freedom where the sleeve and the ring can rotate and translate but the gearwheel can only rotate. Three cases of synchronization process are considered. In the first two cases, the master rotational speed is prescribed throughout the synchronization process while the slave's speed is adapted to the master's. In the third case, both the sleeve and the gearwheel are free to rotate. The sleeve and the ring also move axially during synchronization except during phase 2 (see Figure 2).

Figure 1. Generic synchronizer
 (Irfan, Berbyuk and Johansson, 2015a).

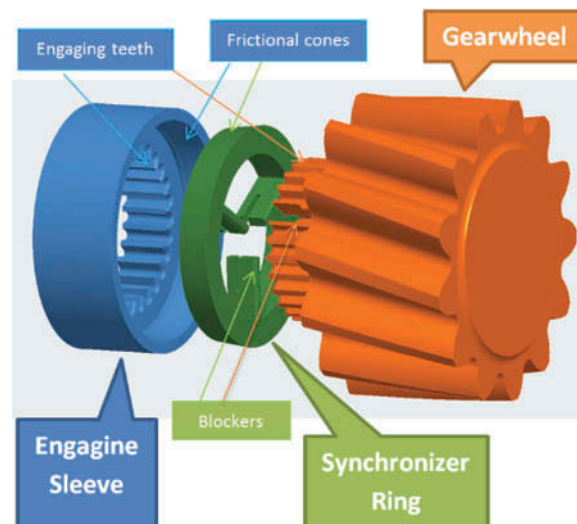
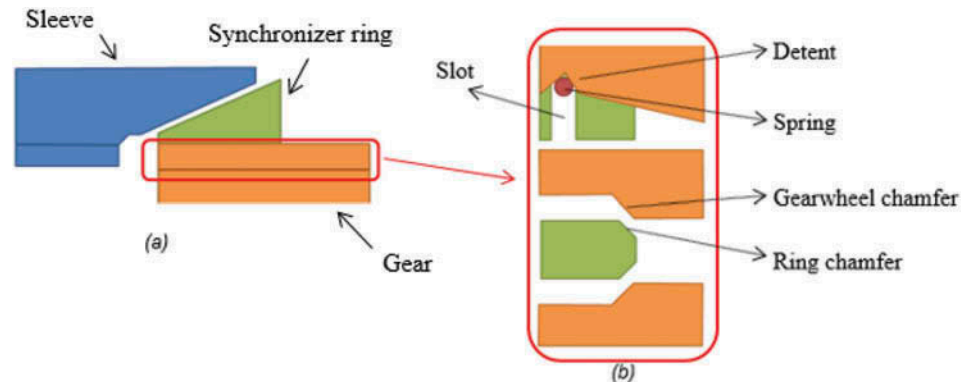


Figure 2. Position of detent, spring, slot, gear chamfer, and ring chamfer before synchronization (Irfan, Berbyuk and Johansson, 2015a).



Kinematics of a synchronization process is presented schematically in Figure 3. In the synchronization process, the sleeve starts to move axially by applying the shift force and the ring gets its axial indexing position during phases 1a and 1b. Lubricant oil is squeezed out from the cones after the ring gets its angular indexing position during phases 1c –1e. In phase 1f, the shift force overcomes the spring axial resistance. During phase 2, movement of the sleeve is blocked due to blocker contact between the ring and the gearwheel. The speed difference reduces between the cones due to friction torque. The system shifts from phase 2 to phase 3 when the sleeve again moves axially. During phases 3a –3c, the sleeve travels axially, passes the blocker contact, and reaches at engagement of the teeth. The sleeve teeth and the gearwheel teeth come in contact during phase 4 until end of the synchronization process as shown in Figure 3.

The vector of generalized coordinates of the system is

$$\mathbf{q} = [x_s, \theta_s, x_r, \theta_r, \theta_g]^T \quad (1)$$

Here, θ_s, θ_r and θ_g are angular coordinates of sleeve, ring, and gearwheel, respectively; x_s and x_r are translational coordinates of the sleeve and ring, respectively. Due to the design of synchronizer, motion of the system is restricted by a set of holonomic kinematic constraints $\Phi(\mathbf{q}, t) = 0$. By introducing λ as the Lagrange multiplier vector (same dimension as Φ), motion of the system is described by a set of differential-algebraic equations (DAE)

$$\begin{cases} \frac{d}{dt} \left(\frac{\partial L}{\partial \dot{\mathbf{q}}} \right) - \frac{\partial L}{\partial \mathbf{q}} + \left[\frac{\partial \Phi}{\partial \mathbf{q}} \right]^T \lambda = \mathbf{Q}^A \\ \Phi(\mathbf{q}, t) = 0 \end{cases} \quad (2)$$

where $L(\mathbf{q}, \dot{\mathbf{q}})$ is the Lagrangian of the system and \mathbf{Q}^A is a vector of generalized forces due to non-conservative applied loads. Vector of non-conservative forces \mathbf{Q}^A is further divided into $\mathbf{Q}^A = \mathbf{Q}_{app}^A + \mathbf{Q}_{fric}^A$, where \mathbf{Q}_{fric}^A are generalized forces arising due to friction between bodies and other losses and \mathbf{Q}_{app}^A are generalized forces due to applied forces arising from external stimuli. For the generic synchronizer under consideration, the DAE is written as follows:

$$\begin{bmatrix} m_s & 0 & 0 & 0 & 0 \\ 0 & I_s & 0 & 0 & 0 \\ 0 & 0 & m_r & 0 & 0 \\ 0 & 0 & 0 & I_r & 0 \\ 0 & 0 & 0 & 0 & I_g \end{bmatrix} \begin{bmatrix} \ddot{x}_s \\ \ddot{\theta}_s \\ \ddot{x}_r \\ \ddot{\theta}_r \\ \ddot{\theta}_g \end{bmatrix} + \left[\frac{\partial \Phi}{\partial \mathbf{q}} \right]^T \lambda = \begin{bmatrix} F_s \\ 0 \\ 0 \\ 0 \\ 0 \end{bmatrix}^{app} - \begin{bmatrix} F_{sf} \\ M_{sf} \\ F_{rf} \\ M_{rf} \\ N_{gf} \end{bmatrix}^{app} - \begin{bmatrix} C_{sa} \text{sign}(\dot{x}_s) \\ C_s \dot{\theta}_s \\ -C_{rp} \text{sign}(\dot{x}_r) \\ C_r \dot{\theta}_r \\ C_g \dot{\theta}_g \end{bmatrix} \quad (3)$$

$$\Phi = \begin{bmatrix} \Phi^{imposed} \\ \Phi^{internal} \end{bmatrix} = 0, \Phi(\mathbf{q}, t)^{imposed} = \theta_s - \omega_s^{pres} t \quad (4)$$

Notations and constraints in Eqs. (3) and (4) are presented in Tables 1 and 2.

Table 1. Internal constraints during subphases of the synchronization

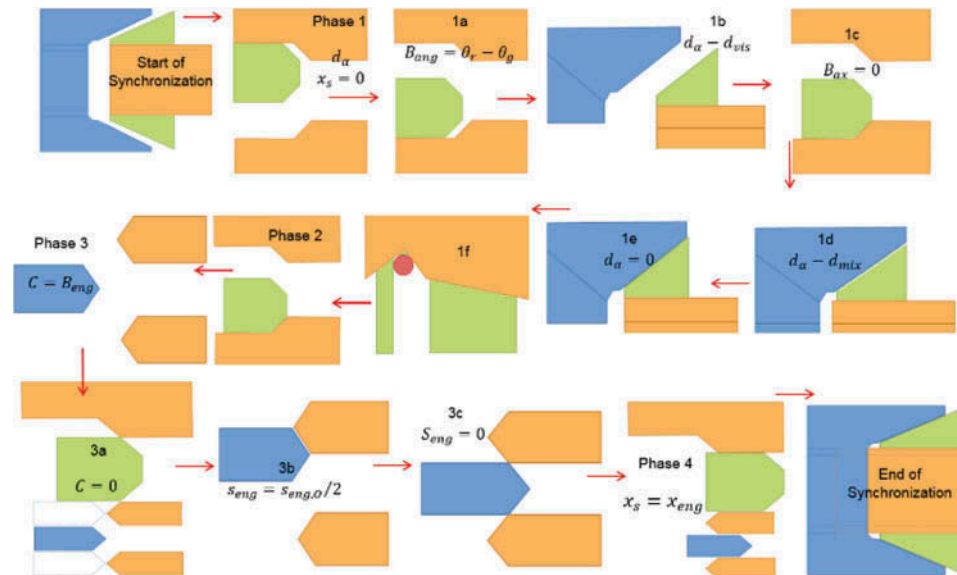
Phase	Constraint: $\Phi(q, t)^{internal} = 0$	Phase	Constraint: $\Phi(q, t)^{internal} = 0$
1a	$[x_r]=0$	2	$\begin{bmatrix} x_r - B_{ax} \\ x_s - x_r - d_{\alpha} \\ \theta_r - \theta_g - B_{ang} \end{bmatrix} = 0$
1b	$\begin{bmatrix} x_r \\ \theta_r - \theta_g - B_{ang} \end{bmatrix} = 0$	3a	$\begin{bmatrix} x_s - x_r - d_{\alpha} \\ \theta_r - \theta_g - B_{ang} - \frac{x_r - B_{ax}}{r_{\beta}} \tan \beta \end{bmatrix} = 0$
1c	$\begin{bmatrix} x_s - x_r - d_{vis} \\ \theta_r - \theta_g - B_{ang} \end{bmatrix} = 0$	3b	$\begin{bmatrix} x_s - x_r - d_{\alpha} \\ \theta_r - \theta_g - B_{ang} - \frac{x_r - B_{ax}}{r_{\beta}} \tan \beta \end{bmatrix} = 0$
1d	$\begin{bmatrix} x_r - B_{ax} \\ x_s - x_r - d_{mix} \\ \theta_r - \theta_g - B_{ang} \end{bmatrix} = 0$	3c	$\begin{bmatrix} x_s - x_r - d_{\alpha} \\ \theta_r - \theta_g - B_{ang} - \frac{x_r - B_{ax}}{r_{\beta}} \tan \beta \end{bmatrix} = 0$
1e	$\begin{bmatrix} x_r - B_{ax} \\ x_s - x_r - d_{\alpha} \\ \theta_r - \theta_g - B_{ang} \end{bmatrix} = 0$	4	$\begin{bmatrix} x_s - x_r - d_{\alpha} \\ \theta_r - \theta_s + \theta_{r-s} \\ \theta_r - \theta_g - B_{ang} + \theta_{g-s} \end{bmatrix} = 0$
1f	$\begin{bmatrix} x_r - B_{ax} \\ x_s - x_r - d_{\alpha} \\ \theta_r - \theta_g - B_{ang} \end{bmatrix} = 0$		

The synchronizer process is complex to understand because of nature of interaction of the bodies. To simplify the understanding of the interaction of each part the synchronization process is divided into several subphases, as shown in Figure 3. Cut views of each subphase in Figure 3

Table 2. Parameters for the synchronization process

Variable	Name	Variable	Name
$m_s = 1.5 \text{ kg}$	Sleeve mass	$m_r = 0.5 \text{ kg}$	Ring mass
$I_g = 0.2 \text{ kgm}^2$	Gear moment of inertia	$I_s = 0.01 \text{ kgm}^2$	Sleeve moment of inertia
$I_r = 0.004 \text{ kgm}^2$	Ring moment of inertia	$r_{\beta} = 0.07 \text{ m}$	Chamfers mean radius
$r_{\alpha} = 0.1 \text{ m}$	Cones mean radius	$d_{vis} = 1 \text{ mm}$	Viscous clearance
$b = 5 \text{ mm}$	Cones contact length	$d_{\alpha} = 2 \text{ mm}$	Cones Initial clearance
$\beta = 60^{\circ}$	Chamfer angle	$h_{min} = 0.1 \text{ mm}$	Mixed friction clearance
$\alpha = 7^{\circ}$	Cone angle	$B_{ang} = 5^{\circ}$	Angle clearance
$C_r = 0.003$	Ring oil splash losses	$\mu_{\alpha} = 0.17$	Cones friction coefficient
$C_g = 5$	Gear oil splash losses	$C_s = 1$	Sleeve oil splash losses
$C_{r\beta} = 0.002$	Ring sliding friction	$C_{sa} = 0.02$	Sleeve sliding friction
$\omega_s = 1000 \text{ rpm}$	Sleeve rotational speed	$\omega_g = 700 \text{ rpm}$	Initial gear rotational speed
\dot{x}_s	Sleeve axial speed	\ddot{x}_s	Sleeve axial acceleration
\dot{x}_r	Ring axial speed	\ddot{x}_r	Ring axial acceleration
$\dot{\theta}_s$	Sleeve rotational speed	$\ddot{\theta}_s$	Sleeve rotational acceleration
$\dot{\theta}_r$	Ring rotational speed	$\ddot{\theta}_r$	Ring rotational acceleration
F_s^{app}	Applied shift force	$\ddot{\theta}_g$	Gear rotational acceleration
θ_s	Sleeve rotational displ.	ω_s^{pres}	Sleeve prescribed speed
$\mu_{\beta} = 0.09$	Blocker friction coefficient	$T_c = \lambda_{cons} \mu_{\alpha} F_s$	Cone Torque (Lovas, 2004) phase 2
$F_{sf} = 16\pi\rho\dot{x}_s \sin(\alpha) r_c \left(\frac{b}{h}\right)^3$		Axial force at viscous friction (Lovas, 2004) phase 1d and 1e	
$M_{sf} = 4\pi\rho\dot{x}_s r_c^3 \omega_s \frac{b}{h} \left(1 - \frac{\omega_g}{\omega_s}\right)$		Torque at viscous friction (Lovas, 2004) phase 1d and 1e	

Figure 3. Phases of the synchronization process (Irfan, Berbyuk and Johansson, 2015a).



show only those sections of the bodies where the contact changes its nature. Detail description is given in Irfan, Berbyuk and Johansson (2015a). Figure 2 shows an example that how the ring and the gear can have internal contact through blockers, detent, and spring.

3. The generic synchronizer performance

A synchronizer performance is modeled by applying the developed mathematical model and numerical algorithm in Irfan, Berbyuk and Johansson (2015a). All input parameters are considered same as in Irfan, Berbyuk and Johansson (2015a) and are shown in Table 2. The sleeve, ring, and gear move to perform the gear shift by engaging the teeth. The generic synchronizer performance diagram obtained from simulation of the synchronizing process for a down shift gear change is presented in Figure 3.

As follows from Figure 4, the sleeve translates because of applying the shift force. The sleeve keeps its rotational speed constant throughout the synchronization process. Before the fluid friction (phase 1c), rotational speed of the gearwheel decreases and rotational speed of the ring increases. The sleeve does not translate during phases 1f and 2 but speed of the gearwheel increases with increasing shift force. From phase 3, the sleeve moves axially again. Engagement of teeth starts before ending phase 3 which complete during phase 4.

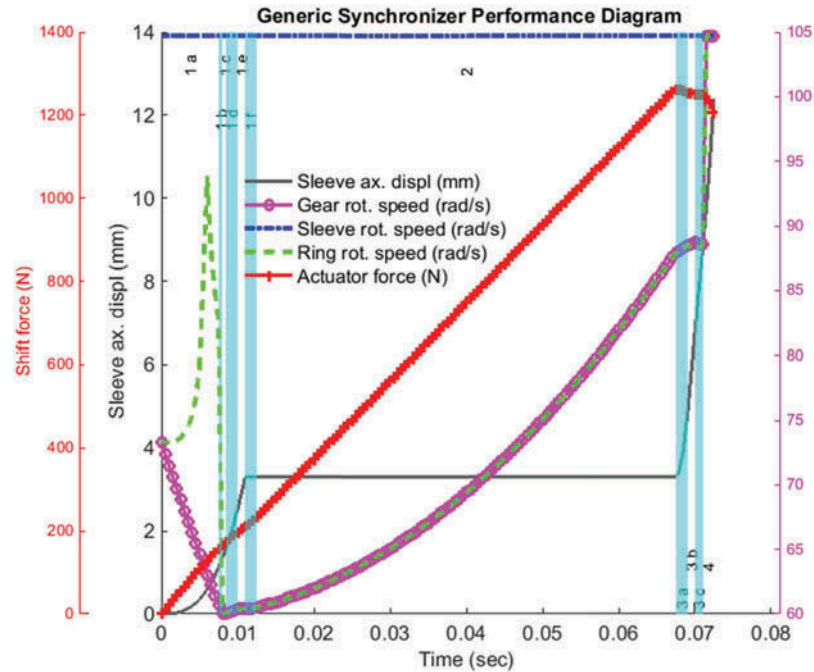
4. Validation

The generic synchronizer depicted in Figure 1 was modified to be able to use available experimental data for model validation. The modified generic synchronizer has cones between the ring and the gear and blocking chamfers are shifted from slave to master side. The kinematics of the synchronizing process of the modified synchronizer is shown in Figure 5.

The shift force is applied on the modified synchronizer to obtain the synchronizer performance. Experimental and simulated results of sleeve axial displacement and gear rotational speed are compared as shown in Figure 6. The results show that synchronizer model developed in Irfan, Berbyuk and Johansson (2015a) is reasonably predicting motion of the synchronizer mechanism.

A brown thick line shows axial movement from test rig and a black thin line shows simulated axial movement of the sleeve. Both lines are close to each other particularly at end of the process. A blue thick line shows speed difference from test rig and a magenta thin line shows simulated speed of the

Figure 4. Generic synchronizer performance diagram.



gearwheel. There is a noticeable gap between the experimental and simulated results and the gap is because of the experimental errors which cannot be adjusted in the simulated model.

5. Sensitivity analysis

One of the main objectives under all circumstances is to shift the gear as quick as possible. But it is also demanded to make the gear shift as smooth as possible.

Figure 5. Kinematics of the modified synchronizer.

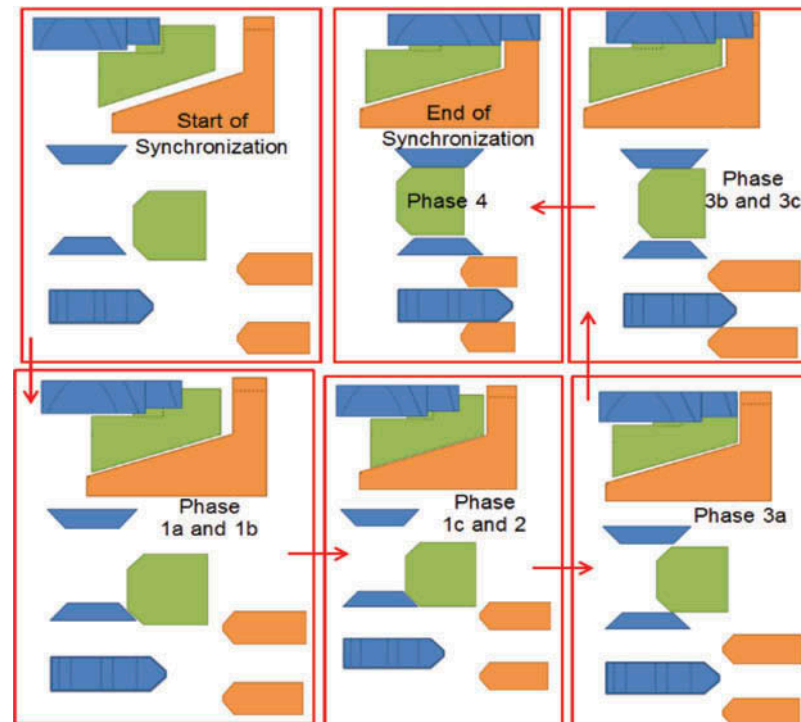
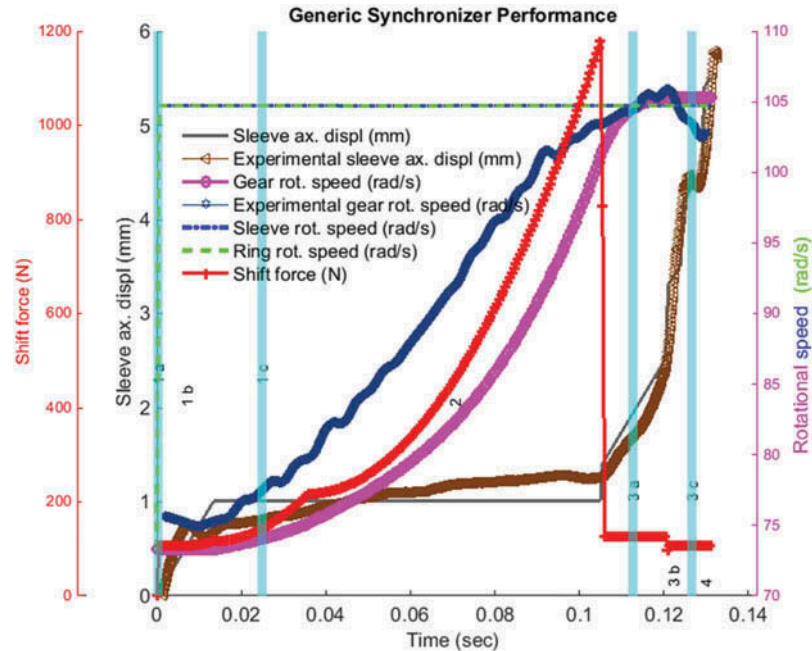


Figure 6. Performance diagram of the modified synchronizer.



To this end, two objectives to measure the generic synchronizer performance are defined as follows:

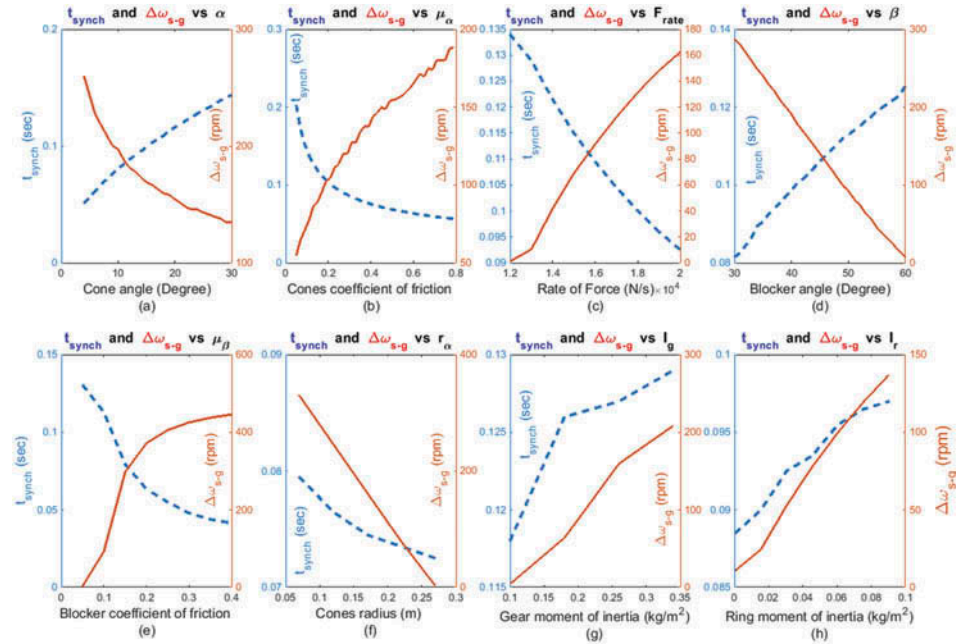
- (1) Synchronization time, (t_{synch}), as a measure of quickness; time from neutral to full engagement of the teeth.
- (1) Speed difference, ($\Delta\omega_{s-g}$), as a measure of smoothness; the difference between rotational speed of the master and the slave at end of phase 2 from where the sleeve starts to move axially again.

Eight parameters of the generic synchronizer are selected as variable parameters to study their influence on the objectives (t_{synch}) and ($\Delta\omega_{s-g}$).

- (2) Rate of applying shift force (F_{rate})
- (3) Cone angle (α)
- (4) Cones coefficient of friction (μ_{α})
- (5) Blocker angle (β)
- (6) Blocker coefficient of friction (μ_{β})
- (7) Mean cones radius (r_{α})
- (8) Moment of inertia of the slave I_s or I_g
- (9) Moment of inertia of the blocker ring (I_r)

The developed model is used to perform sensitivity analysis with eight parameters and two chosen objectives. Synchronization time (t_{synch}) and speed difference ($\Delta\omega_{s-g}$) in Figure 7 (a-f-h) have same trends with respect to each other where t_{synch} and ($\Delta\omega_{s-g}$) increase with increasing gear moment of inertia (I_g) and ring moment of inertia (I_r) but decrease with increasing cone radius (r_{α}). t_{synch} and $\Delta\omega_{s-g}$ have opposite trends in Figure 7 (a-e) with respect to each other where t_{synch} decreases with increasing cones coefficient of friction (μ_{α}), rate of force (F_{rate}) and blocker coefficient of friction (μ_{β}) but increases with increasing cone angle (α) and blocker angle, (β) whereas $\Delta\omega_{s-g}$ increases with increasing μ_{α} , F_{rate} and μ_{β} but decreases with increasing α and β . As it

Figure 7. Individual sensitivity of synchronization time and speed difference with respect to varying parameters.



is follows from Figure 7 t_{synch} and $\Delta\omega_{s-g}$ have conflicting behavior not only within some parameters but also between parameters. A quick synchronizer will be less smooth and a smooth synchronizer will be less quick. A trade-off is obtained between two conflicting objectives in form of Pareto front by applying the optimization technique in the next sections.

In Figure 8, each parameter is analyzed with respect to t_{synch} to illustrate the degree of influence within the given bounds of parametric variation. Change of r_a from 0.07 m to 0.27 m can change t_{synch} from 0.077 s to 0.07 s while change of α from 4° to 30° can change t_{synch} from 0.05 s to 0.15 s. It is predicted that α is more influencing parameter than r_a . In the case where effect of eight parameters on t_{synch} is analyzed; r_a , I_r and I_g are less influencing parameters than α , μ_a , μ_β , β and F_{rate} .

Figure 8. Variation of synchronization time with each parameter.

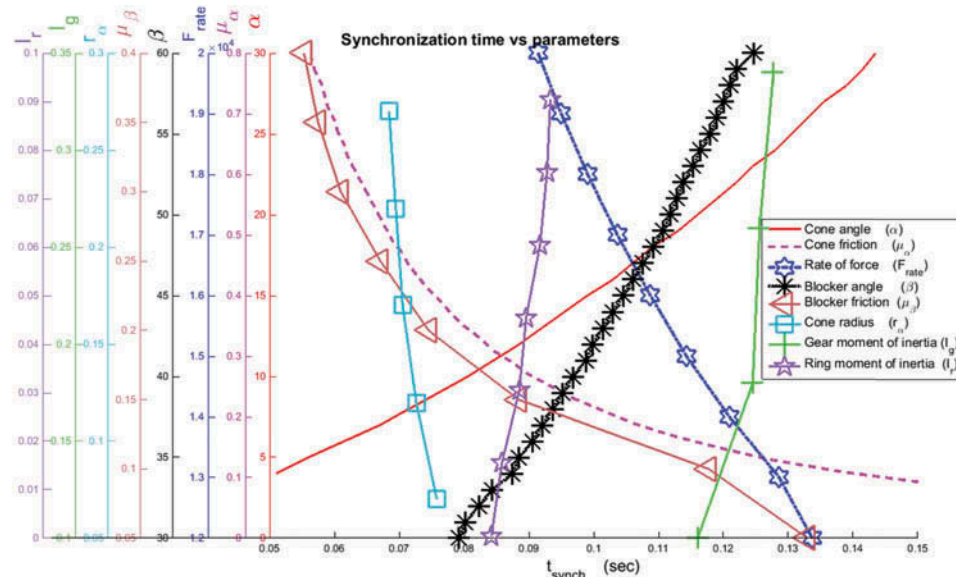


Figure 9 shows an effect of each parameter on $\Delta\omega_{s-g}$. In this local sensitivity analysis I_r , F_{rate} , μ_α , I_g and α have less influence than μ_β , r_α and β because the former parameters can bring less change in $\Delta\omega_{s-g}$ than the later parameters.

6. Pareto optimization

Multi-objective optimization of the synchronizer with respect to the two conflicting objectives, t_{synch} and $\Delta\omega_{s-g}$, is studied. In particular, variations of parameters along the Pareto front is analyzed. To obtain optimal performance of the synchronizer, it is necessary to determine the optimized value of X which gives minimum of the functions $t_{synch}(X)$ and $\Delta\omega_{s-g}(X)$ at the same time subject to DAEs and constraints. Mathematical statement of the bi-objective optimization problem is formulated as follows:

$$\begin{cases} \min_X (t_{synch}(X), \Delta\omega_{s-g}(X)) \\ \tan(\alpha) \geq \mu_\alpha \\ T_c(\alpha, \mu_\alpha, r_\alpha) \geq T_I(\beta, \mu_\beta) \\ X_l \leq X \leq X_u \end{cases}$$

$$\text{where } X = [I_r, I_g, r_\alpha, \mu_\beta, \beta, \alpha, \mu_\alpha, F_{rate}]^T,$$

$$X_l = [0.003, 0.1, 0.1, 0.05, 40, 6, 0.1, 6000]^T$$

$$X_u = [0.01, 0.3, 0.3, 0.25, 60, 15, 0.3, 20000]^T$$

Lower and upper parameters boundaries, X_l and X_u , are reasonably chosen for commercial vehicle.

$$T_c = \frac{F_s \mu_\alpha r_\alpha}{\sin(\alpha)}, \quad T_I = r_\beta F_s \left(\frac{1 - \mu_\beta \tan(\beta)}{\mu_\beta + \tan(\beta)} \right)$$

Here T_c is cone torque and T_I is indexing torque (Irfan, Berbyuk and Johansson, 2015a). The constraint $\tan(\alpha) > \mu_\alpha$ stands for wedging condition and $T_c \geq T_I$ must be hold during gear shifting otherwise the synchronizer will produce clashing of the engaging teeth in every gearshift. The stated Pareto optimization problem is solved by using a Matlab routine of multi-objective optimization with genetic algorithm.

Figure 9. Variation of speed difference with each parameter.

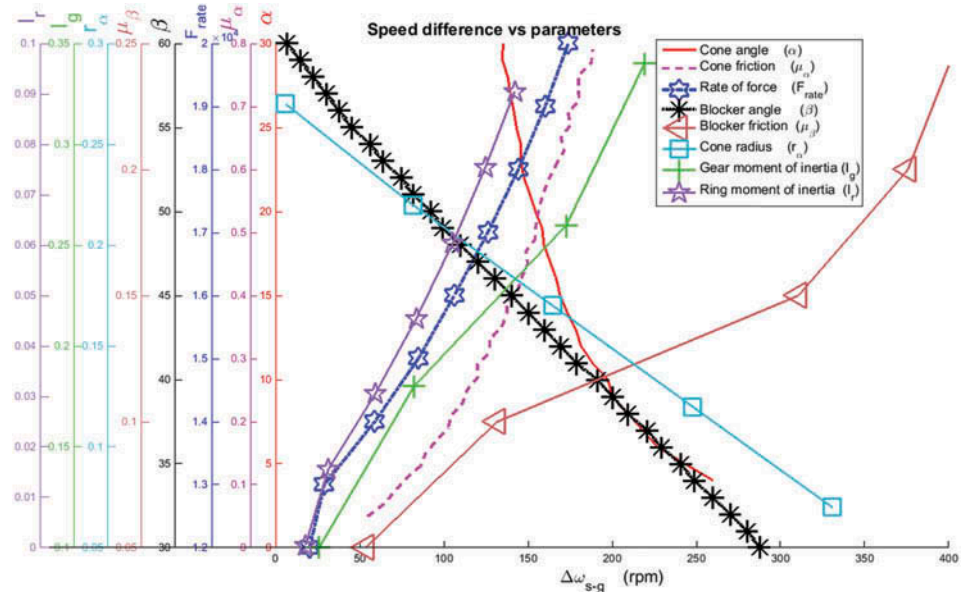


Table 3. 8 cases with different setting of master and slave

Sleeve as a master	Gear as a master	Both slave
Nominal	Nominal	Nominal
Vibrations	Vibrations	Vibrations
Road grade	Road grade	

Eight cases are considered as shown in Table 3 to optimize the synchronization process where sleeve/gearwheel can be considered as master/slave under three operating conditions: nominal, available transmission vibration, and road grade.

7. Results of optimization

7.1. Sleeve as a master

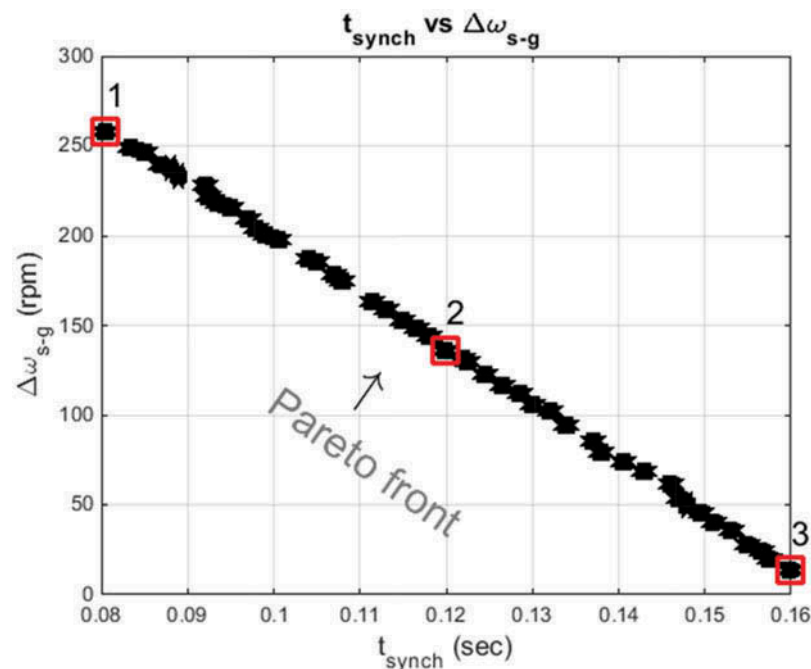
In synchronizer mechanism, different settings of master/slave are possible to support working environment of the transmission line in the vehicle. Initially, as a nominal case sleeve is considered as a master.

7.1.1. Nominal case

In nominal case, the synchronization process is studied without introducing the vibrations and road grade in the mathematical model of the synchronizer. Figure 10 shows the trade-off between t_{synch} and $\Delta\omega_{s-g}$ obtained by solving Pareto optimization. The synchronizer with minimum t_{synch} can be selected from point 1 but $\Delta\omega_{s-g}$ is maximum at the same point. At point 3 the synchronizer has minimum $\Delta\omega_{s-g}$ but has maximum t_{synch} . The synchronizer selected at point 2 illustrate a trade-off values of synchronization time and speed difference.

The synchronizer selected at each point of the Pareto front has corresponding values of the eight parameters. Figure 11 shows variation of the cone angle (r_α) along the Pareto front. r_α has no trend because it goes up and down along the Pareto front from point 1 to point 3.

Figure 10. Pareto front between speed difference and synchronization time.



As shown in Figure 12(h), Pareto sets points for F_{rate} uniformly increases along the Pareto front from point 3 to point 1 but μ_β, β, α and μ_α nonuniformly increase along the Pareto front (see Figure 12(d-g)). Pareto sets points for parameters I_r, I_g and r_α do not have significant trends (see Figure 12(a-c)). It can be concluded that the parameters $\mu_\beta, \beta, \alpha, \mu_\alpha$ and F_{rate} depend more on the quickness-smoothness trade-off of the synchronization process than upon the parameters I_r, I_g and r_α .

Nonuniform behaviors show that small change in considered input parameters of the generic synchronizer can bring a significant change in t_{synch} and $\Delta\omega_{s-g}$ which can be seen by scattering of points in Figure 12 except F_{rate} .

Degrees of influence also depend on percentage change of parameters in optimized range of values. If the parameter with higher degree of influence from Figure 12 has less percentage change, the parameter will not be considered to have higher degree of influence on the objective functions. Percentage changes in input parameters and objectives are chosen to be calculated as follows

$$\% \Delta = \frac{(\text{maximum} - \text{minimum})}{\text{nominal}} \times 100$$

As shown in Figure 13, the percentage change of F_{rate} is higher than the percentage change of $I_r, I_g, r_\alpha, \mu_\beta, \beta, \alpha$ and μ_α . Percentage change in $\Delta\omega_{s-g}$ is higher than percentage change in t_{synch} . From Figures 12 and 13, it can be concluded that $\mu_\beta, \alpha, \mu_\alpha$ and F_{rate} are most influencing parameters. Percentage change of t_{synch} and $\Delta\omega_{s-g}$ shows performance improvement level of the synchronizer. All 8 variable parameters together can decrease $\Delta\omega_{s-g}$ from 258 rpm to 14 rpm and t_{synch} from 0.16 s to 0.08 s.

Figure 14(b) shows variation of objective functions with rate of applied force in optimized range of Pareto front. Side view 01 shows variation of t_{synch} with respect to F_{rate} and side view 02 shows variation of $\Delta\omega_{s-g}$ with respect to F_{rate} . Figure 14(b) is obtained by plotting side view 01 and side view 02 together from Figure 14(a). Because of the highest influencing of parameter F_{rate} trends of t_{synch} and $\Delta\omega_{s-g}$ are uniform.

In Figure 15(d-g) t_{synch} decreases but $\Delta\omega_{s-g}$ increases with increasing $\mu_\beta, \beta, \alpha, \mu_\alpha$ and F_{rate} . In Figure 15(a-c) t_{synch} and $\Delta\omega_{s-g}$ do not have significant trends with increasing I_r, I_g and r_α .

Figure 11. Variation of cone radius along the Pareto front Figure (c).

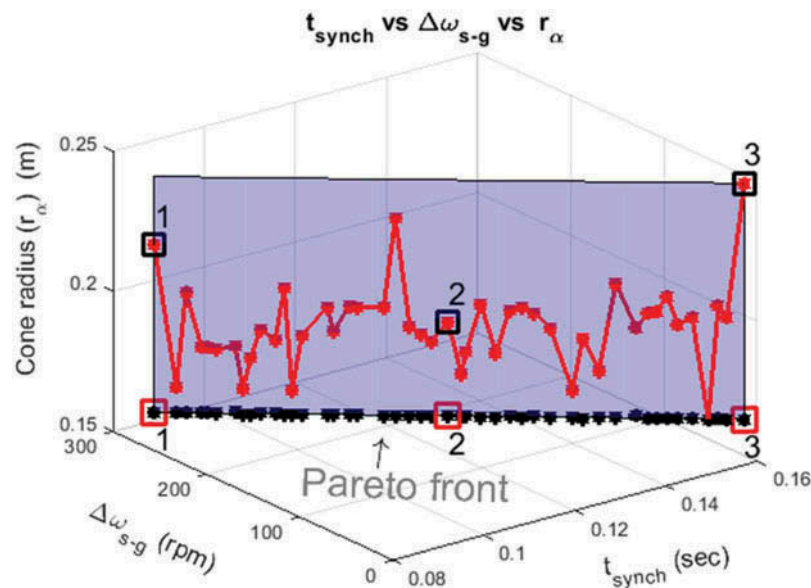
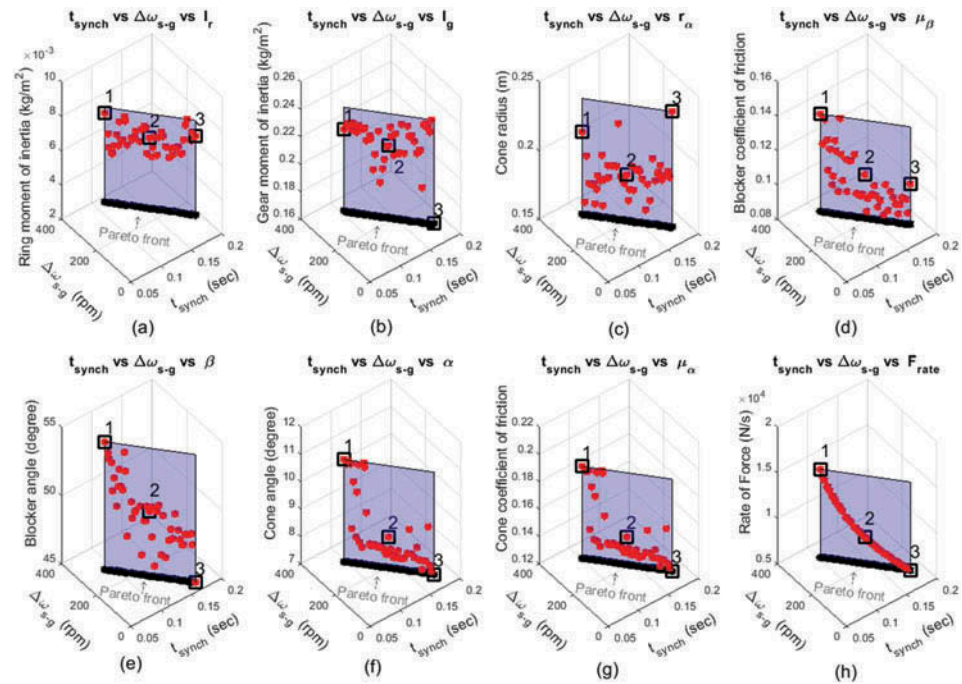


Figure 12. Variation of Pareto sets points of eight parameters along the Pareto front.



A synchronizer with optimized values of the input parameters can be selected from Pareto sets points as shown in Figure 15. Points 1, 2, and 3 of t_{synch} and $\Delta\omega_{s-g}$ in Figure 15 (a-h) show that quicker synchronizer will be less smooth and smoother synchronizer will be less quick because point 1 belongs to 0.0805 sec synchronization time and 258 rpm speed difference with one kind of synchronizer and point 3 belongs to 5 sec synchronization time and 14 rpm speed difference with another kind of synchronizer.

Figure 13. Normalized percentage of input parameters and objectives.

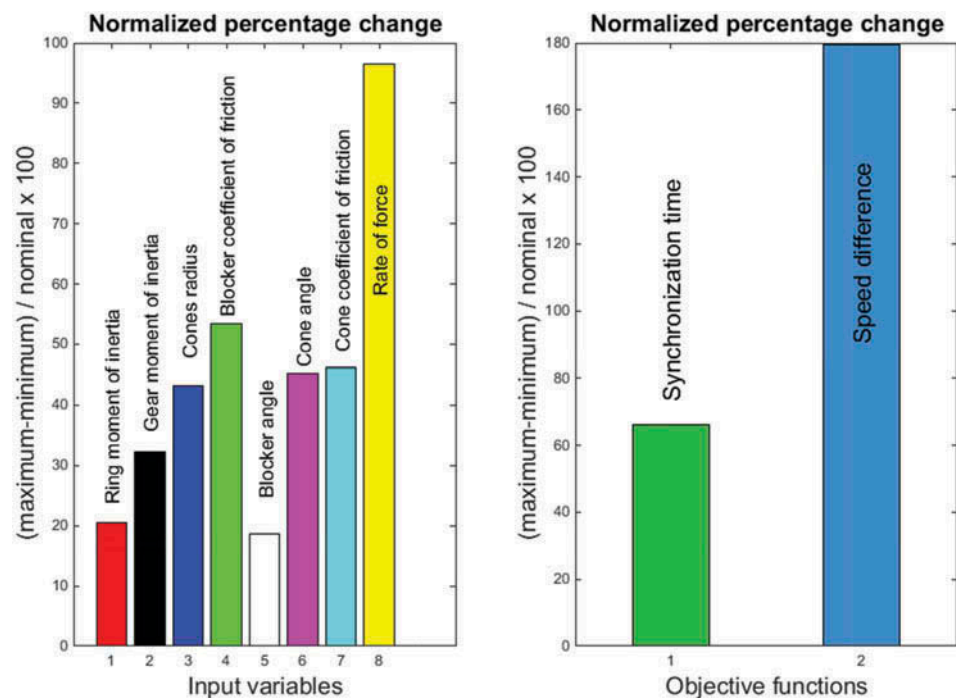
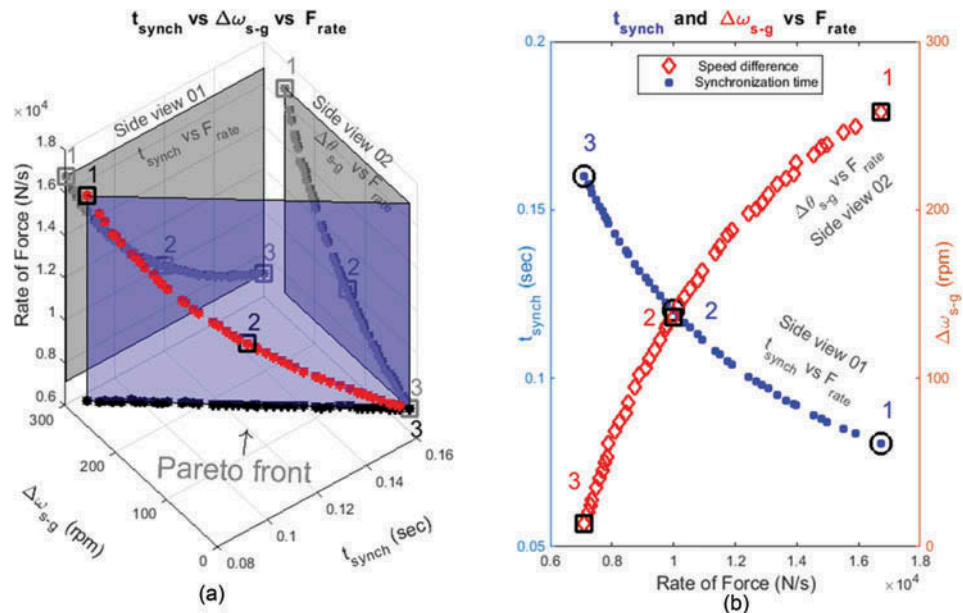


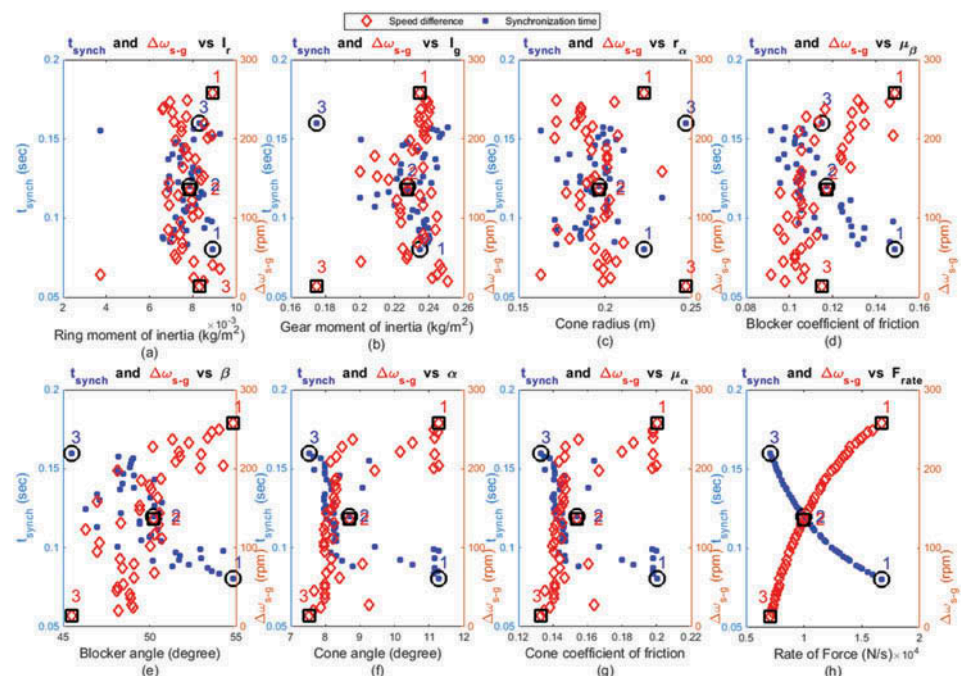
Figure 14. Variation of t_{synch} and $\Delta\omega_{s-g}$ with F_{rate} in optimized range of Pareto front.



In Figure 15(f,g), t_{synch} and $\Delta\omega_{s-g}$ have most of the points almost along a vertical line at a particular value of the parameters α and μ_a . This kind of feature shows that α and μ_a can be ignored from selection process of the optimized synchronizer by adjusting only remaining 6 parameters. In the same way there are some points in Figure 15 which are almost along the horizontal line having same value of t_{synch} and $\Delta\omega_{s-g}$ but having different values of the parameters. To select a synchronizer with same quickness (t_{synch}) and smoothness ($\Delta\omega_{s-g}$) there are several combination of parameter values that give the same performance.

In the area between points 3 and 2 in Figure 15(h) t_{synch} and $\Delta\omega_{s-g}$ are more rapidly vary than in the area between points 2 and 1. Half of total changes in t_{synch} and $\Delta\omega_{s-g}$ are between 7867 N/s

Figure 15. Variation of objectives with parameters in the optimal range of Pareto front.



and 10,000 N/s corresponding to point 3 and point 2. Half of total changes in t_{synch} and $\Delta\omega_{s-g}$ are between 10,000 N/s and 16,741 N/s corresponding to points 2 and 1. The synchronizer selected in the right side area between points 1 and 2 is more expensive than the synchronizer in the left side area between points 2 and 3 because change of F_{rate} in the right side area is 6741 N/s and change of F_{rate} in the right side area is 2133 N/s.

7.1.2. Road grade

To take into account the road grade on the synchronizer mechanism performance, the computational model was updated by applying additional resisting torque at synchronizer. It is assumed that the resisting torque is due to the following forces: tire rolling resistance (F_{roll}), air drag force (F_{air}) and gravity induced force (F_{grav}) (Sahlholm & Johansson, 2010; Stenvall, 2010).

$$T_{res} = (F_{roll} + F_{air} + F_{grav})r_{tire}$$

$$T_{res} = (C_R W \cos(\vartheta) + 0.5 C_D \rho A_v v^2 + W \sin(\vartheta))r_{tire} \quad (5)$$

where T_{res} -resisting torque considered at synchronizer, W -vehicle weight, C_R - rolling resistance coefficient, C_D -air drag coefficient, ρ - air density, A_v -vehicle front area, r_{tire} -tire radius, ϑ - angle on road grade, and v -vehicle speed. The parameter values for road grade are given in Table 4. Because it is considered that the master part of the synchronizer is connected with wheels of vehicle through output shaft therefore T_{res} is applied on the sleeve which is a master in this case. The master loses its rotational speed because of slowing down of vehicle in a road grade case with angle ϑ :

$$\vartheta = \tan^{-1}(h/d)$$

Here, h is vertical displacement of the road and d is horizontal displacement of the road. If the slope is given in percentage, the ϑ can be written as

$$\vartheta = \tan^{-1}(\% \text{ slope}/100)$$

The imposed constraint on the master is

$$\Phi(\mathbf{q}, \mathbf{t})^{imposed} = \theta_s - \omega_s^{pres} t - \omega_{res} t$$

where ω_{res} is the speed because of the road grade and obtained from T_{res} .

Some results of Pareto optimization and sensitivity analysis of synchronizer mechanism performance with effect of road grade are presented in Figure 16–20. In total, 100% road grade is studied to see the effect on the synchronizer performance. In Figure 16 generic synchronizer performance is similar to Figure 4 except the sleeve continuously losses its rotational speed because of the road inclination. Pareto front goes down with increasing road grade as shown in Figure 17. Pareto front decreases more in t_{synch} than in $\Delta\omega_{s-g}$.

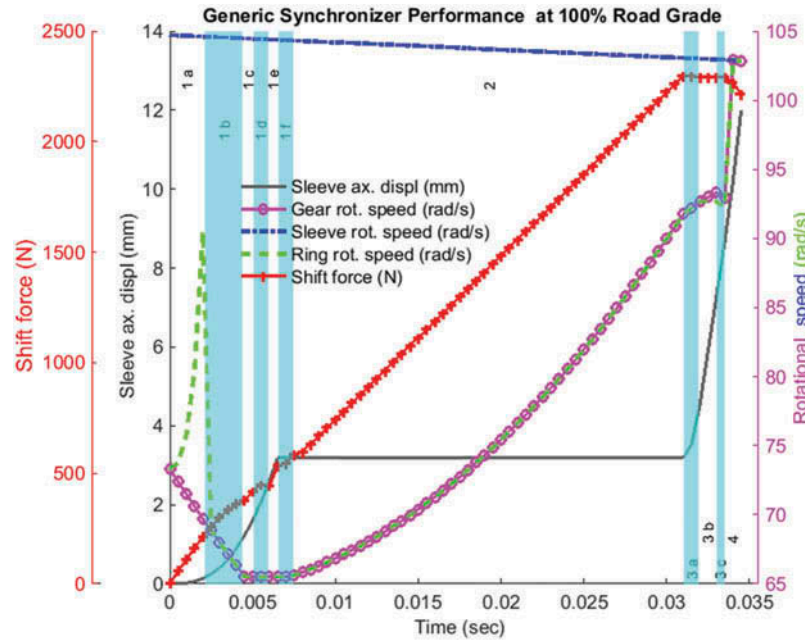
In Figure 17(e–h) Pareto sets points almost have a uniform trend with increasing β , α , μ_α and F_{rate} but in (b,d) Pareto sets points almost have nonuniform trend with increasing I_g and μ_β . In (a,c) Pareto sets points do not have significant trends with increasing I_r and r_α .

In the case of road grade β , α , μ_α and F_{rate} are more influencing than I_r , I_g , r_α and μ_β because of the uniform trend. Pareto sets Points of I_r , I_g , r_α and μ_β are more scattered than Pareto sets points of β , α , μ_α and F_{rate} . As shown in Figure 17(e–g) β , α and μ_α are more influencing parameters at lower

Table 4. Parameters values for road grade

	W (N)	C_D	ρ (kg m ³)	A_v (m ²)	v (km/h)	r_{tire} (m)
0.0076	49,000	0.9	1.2	4.94	85	0.43

Figure 16. Generic synchronizer performance diagram at 100% road grade.



values than at higher values. For example μ_α increases from 0.1 to 0.19 with few Pareto sets points and after μ_α stays around 0.19 with many Pareto sets points. In similar manner in (a) I_r is more influencing parameter at higher value than at lower value.

As shown in Figure 18 percentage changes of α , μ_α , r_α , μ_β , and F_{rate} are higher than percentage changes of I_r , I_g and β . The higher percentage change cannot endorse the degree of influence from Figure 19 because increase in values of the parameters is very small.

Figure 17. Pareto fronts with varying road grade.

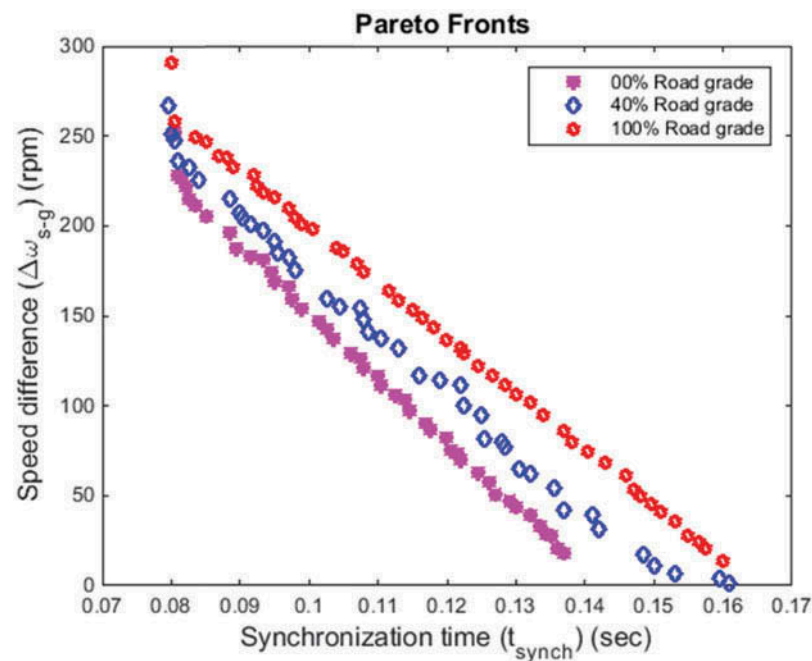
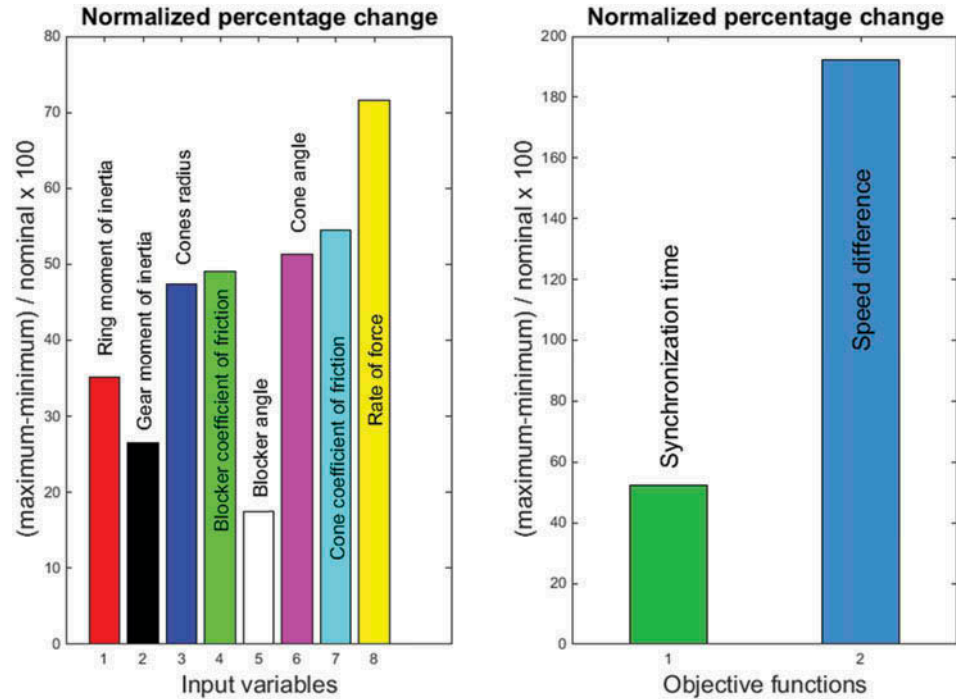


Figure 18. Normalized percentage change of input parameters and objectives.



It is concluded that to keep the synchronizer in the optimized performance range during road grade α , μ_α , r_α , μ_β , and F_{rate} are important parameters to consider in addition to other influencing parameters.

Higher value of μ_α during road grade condition can help to keep the optimal performance of the synchronizer same as during the nominal case.

Percentage change in $\Delta\omega_{s-g}$ is higher than percentage change in t_{synch} . During road grade the synchronizer is smoother than the nominal case.

Figure 19. Variation of Pareto sets points of eight parameters along objectives at 100% road grade.

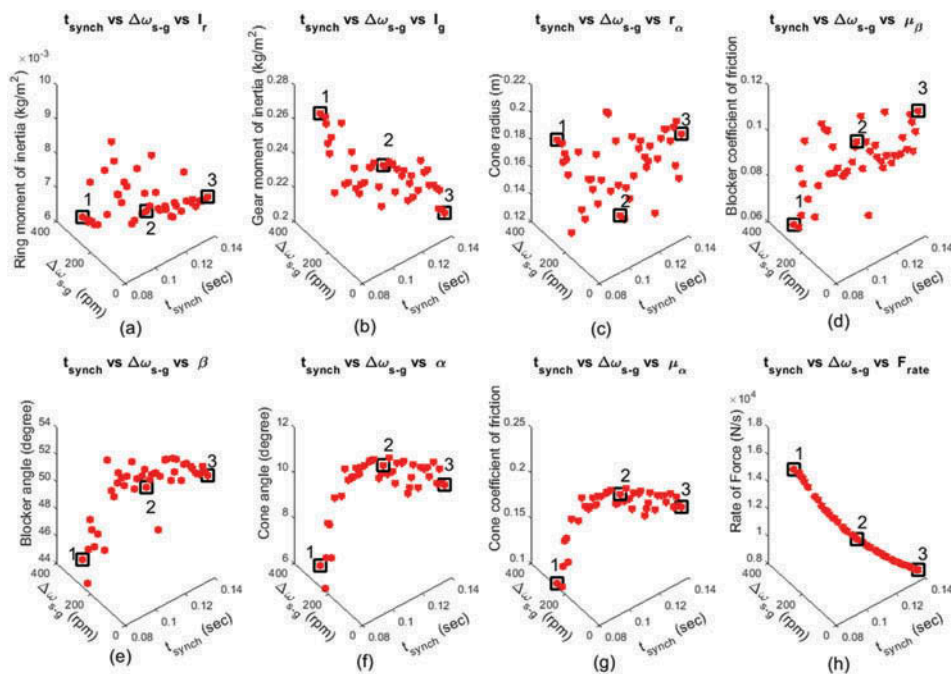
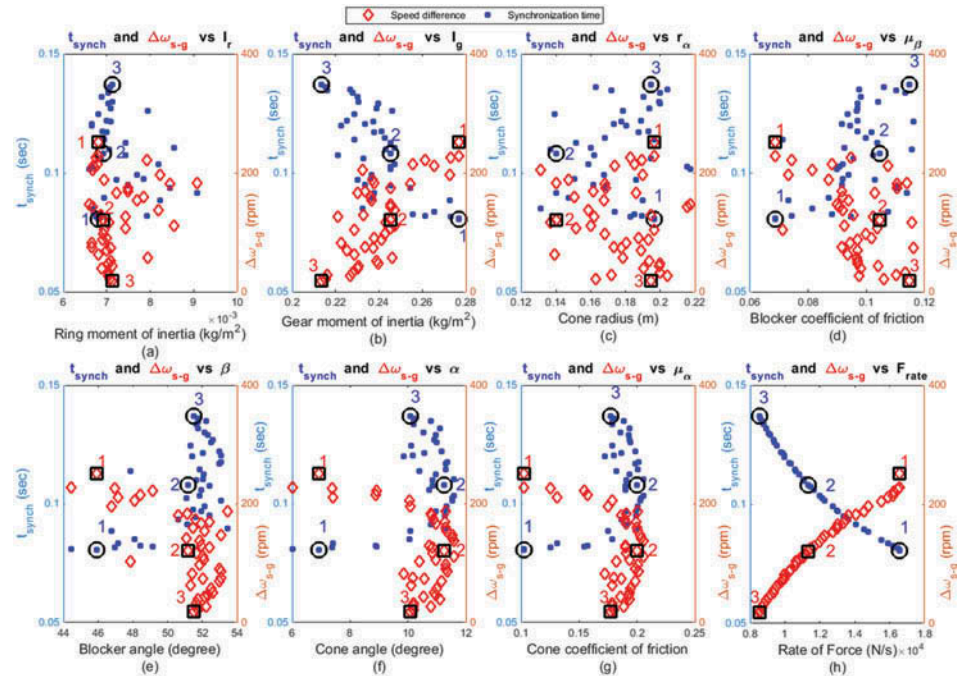


Figure 20. Variation of objectives with parameters at 100% road grade.



In Figure 20(h), Pareto sets points of t_{synch} decrease uniformly but Pareto sets points of $\Delta\omega_{s-g}$ increase uniformly with increasing F_{rate} . In (e-g) Pareto sets points of t_{synch} and $\Delta\omega_{s-g}$ have opposite trends with increasing β , α and μ_α than those of F_{rate} . β , α and μ_α not only have lower rate of change but also stay at a certain value. For example t_{synch} and $\Delta\omega_{s-g}$ of μ_α varies up to almost 0.17 and after μ_α almost stays at 0.17. In (a-d) trends in I_r , I_g , r_α and μ_β are not clear because of scattering of the points.

An optimal performance synchronizer at 100% road grade with optimized values of the input parameters can be selected from Pareto sets points as shown in Figure 20. In Figure 20(a-h), the synchronizer selected between crossing point and point 1 has almost higher quickness and lower smoothness but synchronizer selected between crossing point and point 3 has lower quickness and higher smoothness.

In Figure 20, total span of t_{synch} is shifted down a little than the nominal case while $\Delta\omega_{s-g}$ stayed at almost same level at 100% road grade. Because of slower rate of change in t_{synch} and $\Delta\omega_{s-g}$ the area between point 3 and point 2 increased and the area between point 2 and point 1 decreased. It can be seen that crossing point of t_{synch} and $\Delta\omega_{s-g}$ in Figure 15 is at point 2 and in Figure 20 the crossing point is shifted towards left of point 2.

Because of scattering of points and having insignificant trend, with same smoothness and quickness of synchronizer, more than one combination of values of the parameters I_r , I_g , r_α and μ_β can be selected. In Figure 20 (e-g), most of the points are around a vertical line that shows at fixed value of β , α and μ_α in range of the vertical line the synchronizer can be selected with different t_{synch} and $\Delta\omega_{s-g}$ just only adjusting the values of I_r , r_α , μ_β , I_g and F_{rate} . Most of the points in Figure 20 (a-g) are around the horizontal line that shows at same value of t_{synch} and $\Delta\omega_{s-g}$ more than one value of I_r , r_α , μ_β , I_g , β , α and μ_α can be selected but there is no more options than a single value while choosing F_{rate} because of the uniform trend.

7.1.3. Transmission vibrations

A prominent problem in synchronizer design is the case of transmission vibrations. To study the effect of transmission vibration on synchronizer performance it is assumed that the sleeve

rotational speed is subject to periodic excitation. Therefore, we here study the effect of a periodic variation of the master rotational speed as follows:

$$\dot{\theta}_s^{vib} = \omega_s^{pres} + A_{amp} \sin(2\pi ft + \varphi) \quad (6)$$

where $\dot{\theta}_s^{vib}$ is sleeve rotational speed induced vibrations, $\dot{\theta}_s$ sleeve rotational speed, A_{amp} is amplitude of speed vibrations in rad/s, f is frequency in Hz, t is time in sec and φ is phase of the vibrations in rad. With CLF to get the synchronization performance diagram the imposed constraint in the mathematical model is written as

$$\Phi^{imposed} = \omega_s^{pres} t - \frac{A_{amp}}{2\pi f} \cos(2\pi ft + \varphi)$$

The synchronizer performance in Figure 21 is similar to Figure 4 except the sleeve which has rotational speed with vibrations.

As shown in Figure 22 Pareto fronts in the case of transmission vibrations with a fixed phase shift have jumps with increasing frequency but at a 100-Hz frequency the jumps disappear again. The bifurcation (jumps) in the Pareto fronts is due to vibrating nature of the sleeve rotational speed. Let's consider the shift force which meets at end of phase 2 near trough of ω_s as shown in Figure 21. If F_{rate} is considered to increase, the shift force at end of phase 2 will meet $\dot{\theta}_s$ at left of trough. But if F_{rate} continues to increase, the shift force cannot meet $\dot{\theta}_s$ at crest even further cannot meet $\dot{\theta}_s$ between crest and trough because of vibrating nature of $\dot{\theta}_s$.

As shown in Figure 23, percentage changes of $I_r, r_\alpha, \alpha, \mu_\alpha, \mu_\beta$ and F_{rate} are higher than percentage changes of I_g and β . The average percentage changes of $I_r, r_\alpha, \alpha, \mu_\alpha, \mu_\beta$ and F_{rate} are also higher than theirs corresponding percentage changes in the nominal case that shows the higher variability of the parameters in the case of transmission vibrations than in the nominal one.

Figure 21. Generic synchronization performance diagram with vibration.

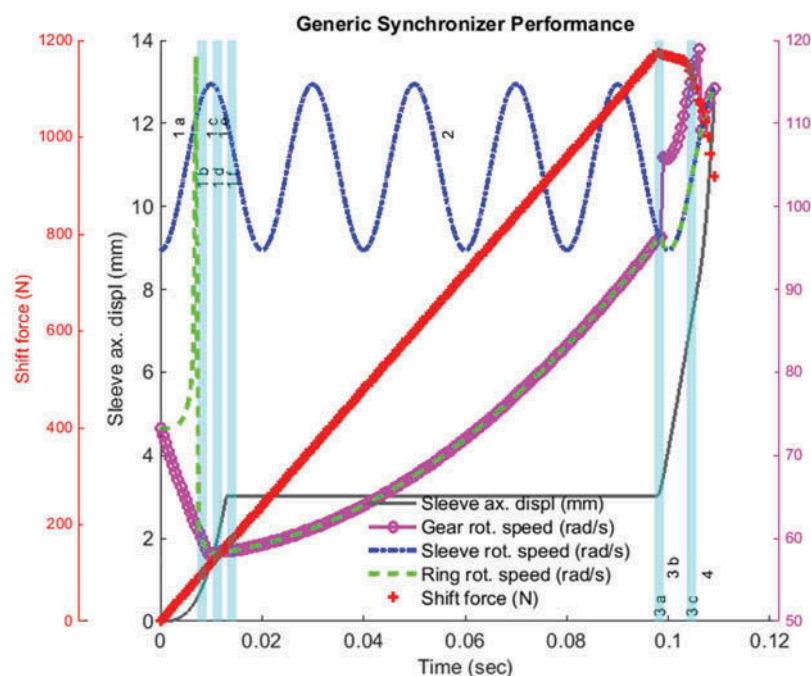
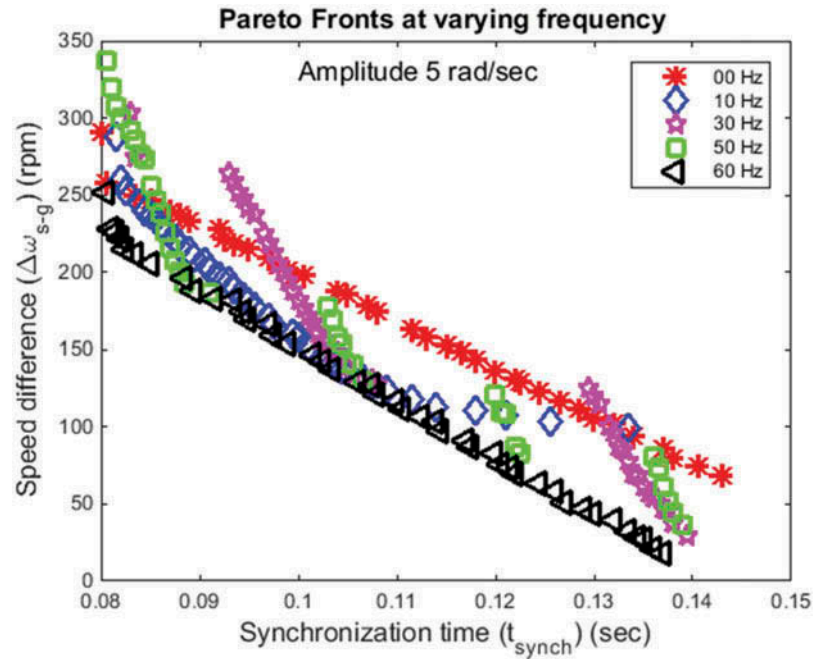


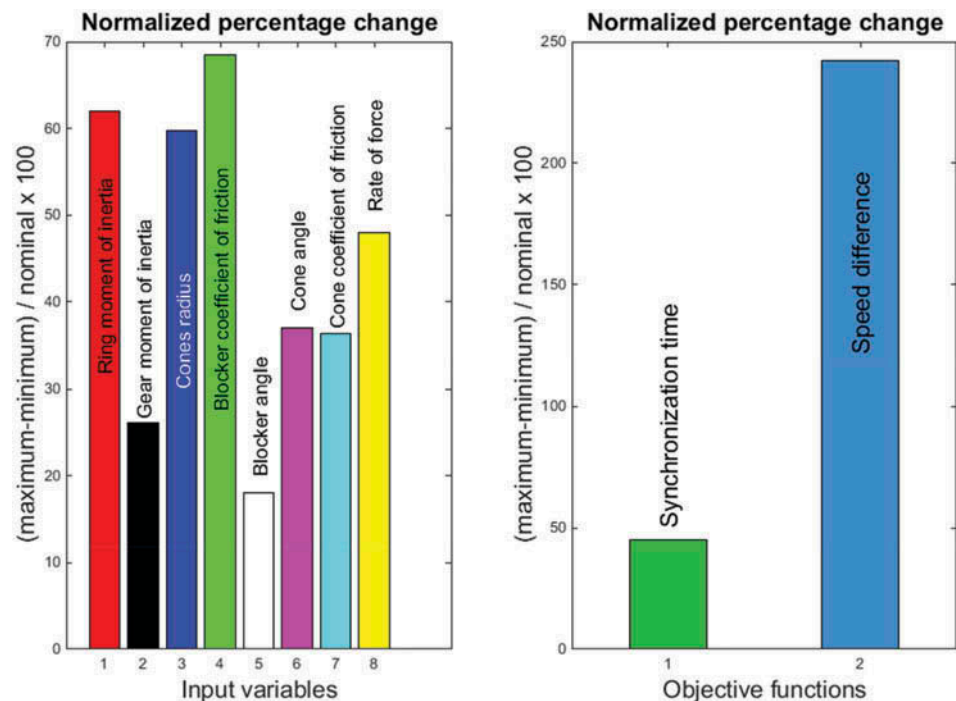
Figure 22. Pareto fronts at transmission vibrations with varying frequency.



Percentage change of F_{rate} is less in the case of vibration than in nominal case that shows F_{rate} is the main agent to determine the trade-off between objectives in the case of different operating conditions.

Percentage change in $\Delta\omega_{s-g}$ is higher than percentage change in t_{synch} but less than the nominal case that shows by introducing the vibrations with higher frequency will make the performance of synchronizer more smoother.

Figure 23. Normalized percentage change of input parameters and objectives.



In Figure 24 (c,e,f,h), Pareto sets points have almost trends with increasing r_α , β , α and F_{rate} . In (a, b,d,g), Pareto sets points do not have significant trends with increasing values of I_r , I_g , μ_β and μ_α . Pareto sets Points of I_r , I_g , μ_β , β , α and μ_α are more scattered than Pareto sets points of r_α and F_{rate} . Because of scattering of the points synchronizer has more than one option to select the values of I_r , I_g , μ_β , β , α and μ_α for the same amount of quickness and smoothness. There are also some missing areas in trends of the Pareto sets points of the parameters due to vibrating nature of $\dot{\theta}_s$.

In Figure 25(c,e,f,h), Pareto sets points of t_{synch} decrease with increasing r_α , β , α and F_{rate} , while Pareto sets points of $\Delta\omega_{s-g}$ increase with increasing r_α , β , α and F_{rate} . In (a,b,d,g), Pareto sets points of t_{synch} and $\Delta\omega_{s-g}$ do not have significant trends with increasing values of I_r , I_g , μ_β and μ_α . Figure 25(c) shows that r_α has no effect on the synchronizer performance during vibrations.

The area belongs to the synchronizer with lower smoothness and higher quickness between the points 2 and 1 is larger than area of the synchronizer with higher smoothness and lower quickness between the points 2 and 3. In Figure 25(h), there are four set of points of $\Delta\omega_{s-g}$ and the sets are almost vertical. Let's consider the set containing point 2 where F_{rate} can be taken as $1.2 \cdot 10^4$ N/s but $\Delta\omega_{s-g}$ changes from 140 rpm to 180 rpm. There is also the similar consideration in Figure 25(a-g). If the selected synchronizer has to be within the range of any set of points as mentioned above, some of the parameters can be ignored from the selection process of the parameters value.

In Figure 26, Pareto fronts decrease with increasing amplitudes of transmission vibrations. The generic synchronizer can perform better at higher amplitude than at lower amplitude of the vibrations. These results depend upon the phase shift.

As shown in Figure 27, percentage change of I_r , μ_β , β and F_{rate} is higher than percentage change of r_α , I_g , α and μ_α . With increasing amplitude changes in the parameters I_r , μ_β , β and F_{rate} are higher than in the nominal case to optimize the synchronization performance.

In Figure 28(h), Pareto sets points increase significantly with increasing F_{rate} . In (a-g) Pareto sets points do not have a significant trends with increasing α , μ_α , μ_β , β , I_g , I_r and r_α . In the case of transmission

Figure 24. Variation of Pareto sets points of parameters at vibrations with 50 Hz frequency.

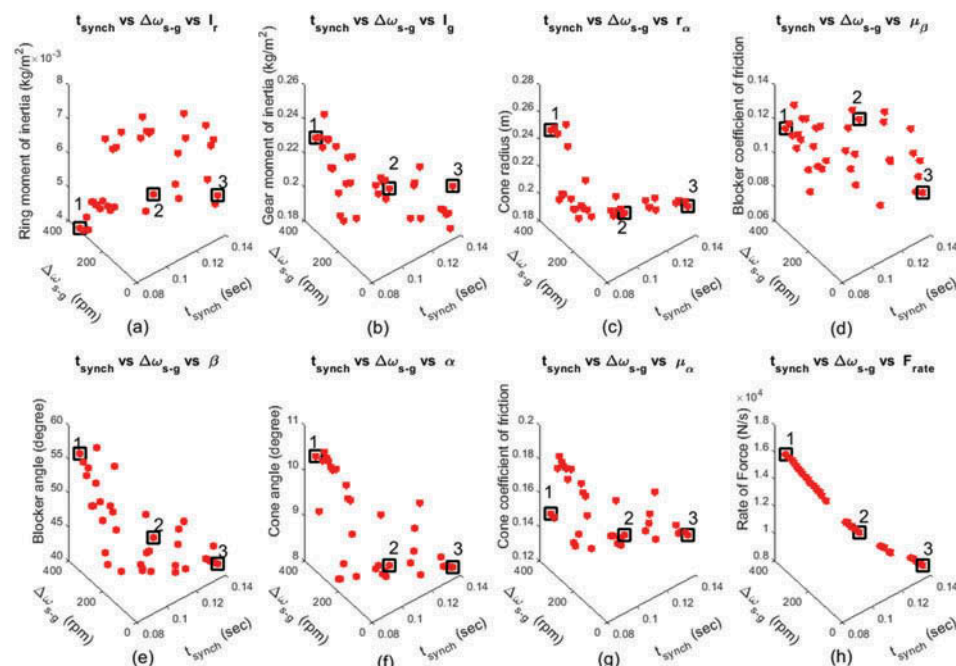
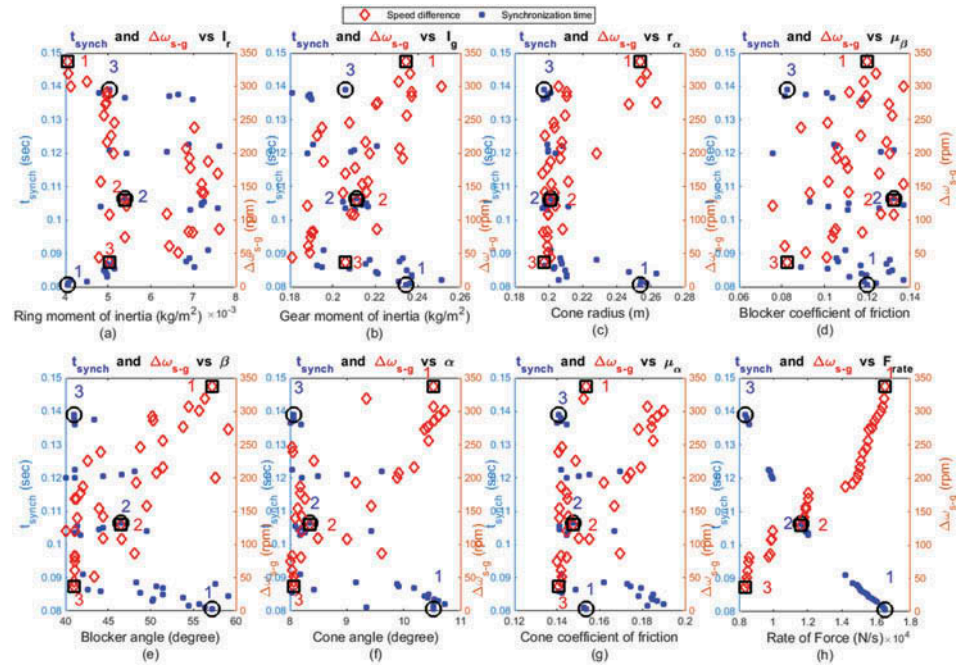


Figure 25. Parameters with objectives in the optimal range with 50 Hz frequency.



vibrations with changing amplitude the parameters $\alpha, \mu_\alpha, \mu_\beta, \beta, I_g, I_r$ and r_a have almost same level of variability. There is also a bifurcation because of vibrating nature of the sleeve rotational speed.

In Figure 29(h), Pareto sets points of t_{synch} decrease but Pareto sets points of $\Delta\omega_{s-g}$ increase with increasing F_{rate} . In (a–g) Pareto sets points of t_{synch} and $\Delta\omega_{s-g}$ do not have significant trends with increasing $\alpha, \mu_\alpha, \mu_\beta, \beta, I_g, I_r$ and r_a .

Figure 26. Pareto fronts at transmission vibrations with varying amplitude of speed.

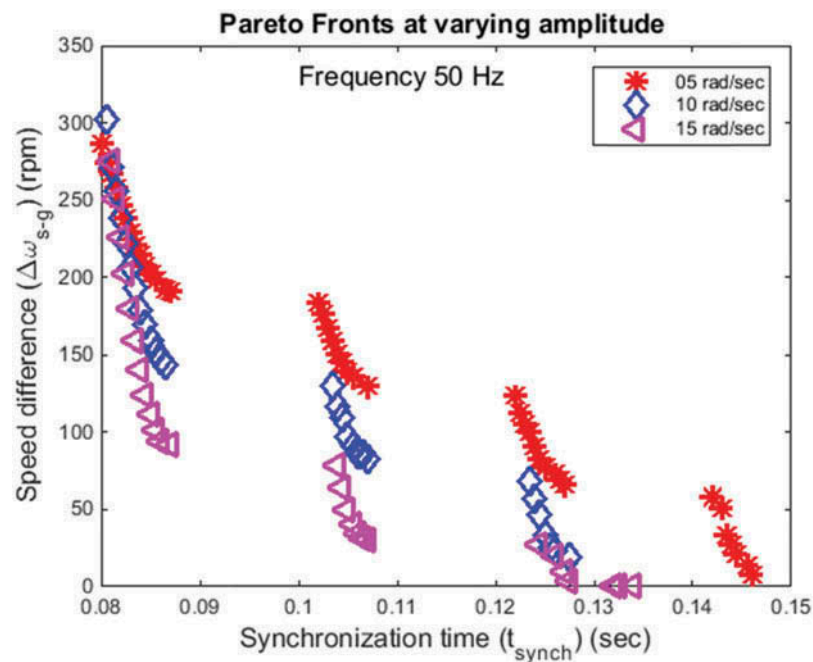
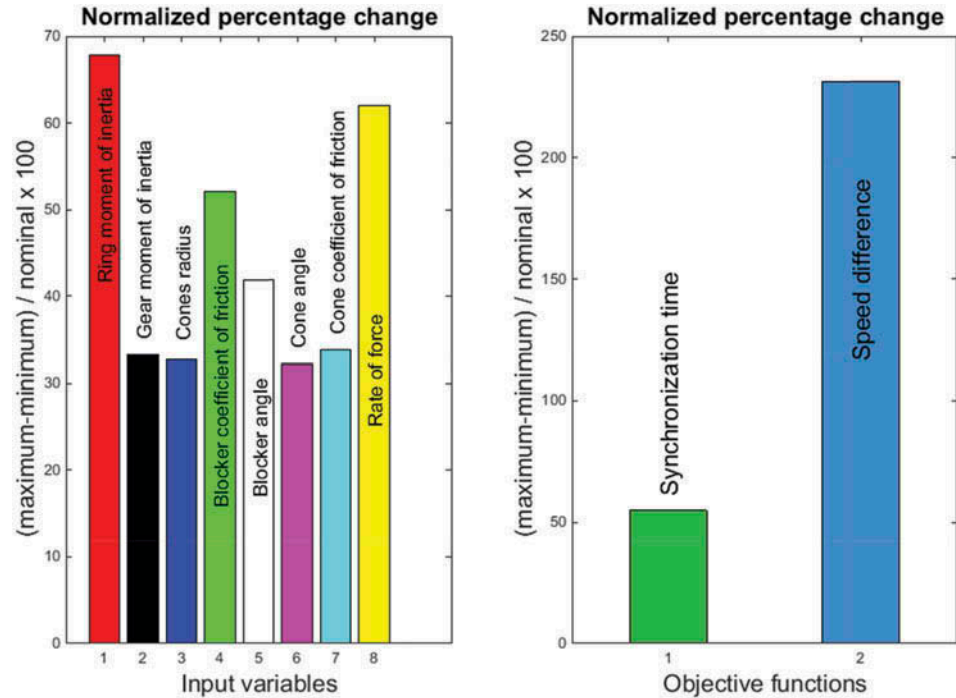


Figure 27. Normalized percentage change in input parameters and objectives.



Bifurcation in the case of increasing amplitude is more than in the case of increasing frequency. There are three sets of points because of bifurcation in Figure 29. In each set points of t_{synch} tend to be horizontal and points of $\Delta\omega_{s-g}$ tend to be vertical in Figure 25(b,c,f,g,h).

It is concluded that the most prominent parameters to control the synchronizer performance can be found by analyzing the Pareto optimization results through a different perspective. In this perspective of analyses trends of Pareto sets points are found along Pareto front which is a trade-

Figure 28. Variation of Pareto sets points of parameters along objectives at 5 rad/sec amplitude.

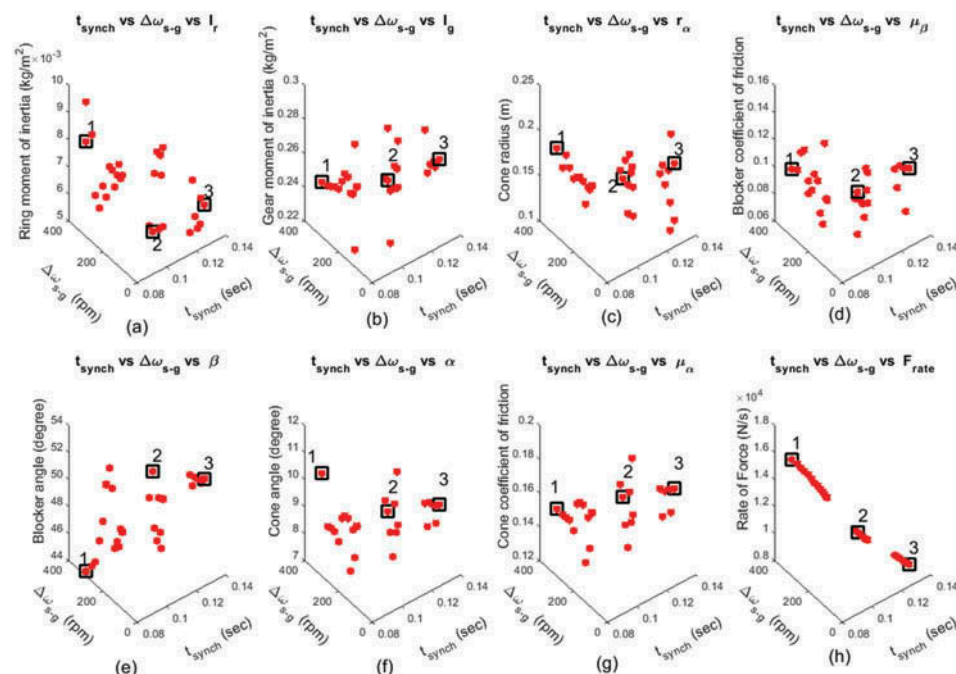
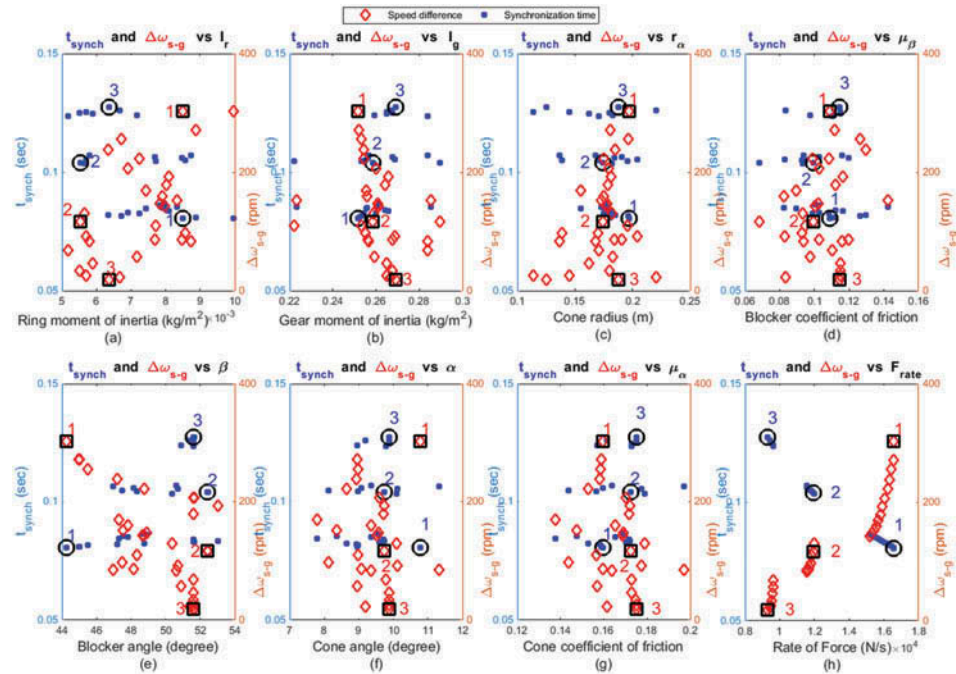


Figure 29. Parameters with objectives in the optimal range at 5 rad/sec amplitude.



off between two conflicting objectives, percentage change of parameters are calculated and behavior of objective functions is studied along the Pareto sets points.

At the nominal condition $\mu_\beta, \beta, \alpha, \mu_\alpha$ and F_{rate} have higher degree of influence than r, I_g and I_r at road grade condition $r, \mu_\beta, \beta, \mu_\alpha$ and F_{rate} have higher degree of influence than α, I_g and I_r and at vibration condition $I_r, \mu_\beta, \alpha, \mu_\alpha$ and F_{rate} have higher degree of influence than β, r, α and I_g . In three conditions μ_α, μ_β and F_{rate} are common which have higher degree of influence than other parameters. So it is concluded with the setting of sleeve as a master that the synchronizer performance can be controlled by varying just the parameters of higher degree of influence which are the following:

7.2. Gearwheel as a master

In the case of split gear in the front of the gearbox, the split synchronizer gearwheel is connected with wheels while the sleeve is connected towards the disengaged clutch which is a case of gearwheel as a master. To see effect of the master/slave setting in this case the gearwheel is considered as a master and the sleeve is considered as a slave.

7.2.1. Nominal case

The synchronizer performance diagram is obtained without road grade and vibration conditions.

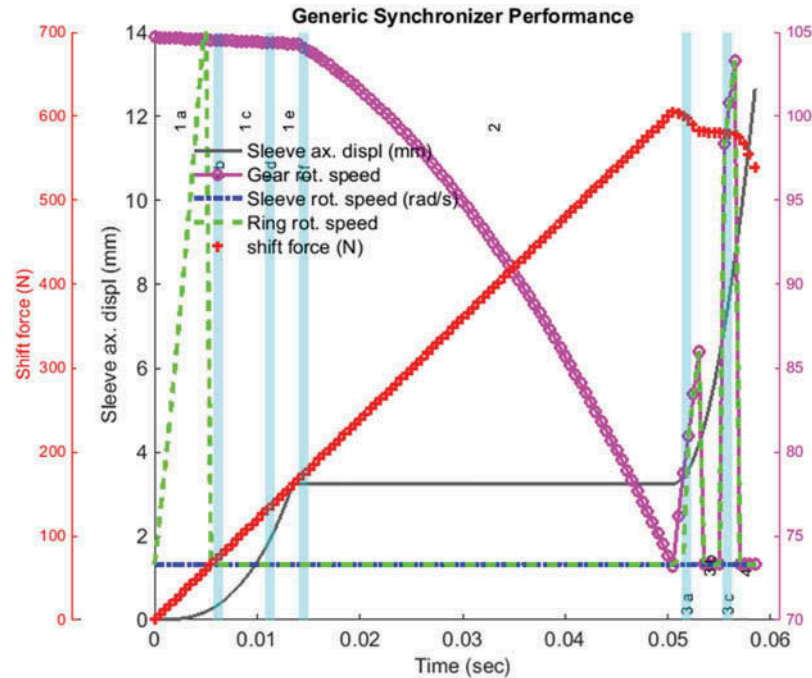
Figure 30 shows the generic synchronizer performance during upshift where gearwheel is considered as a master and sleeve is considered as a slave.

Because the sleeve has less moment of inertia, t_{synch} is less than the case where the sleeve is considered as a master. The sleeve will get a rotational turn to proceed further in axial direction for engagement during phase 3 as shown in Figure 30.

For the cases where gearwheel is considered as a master, upper and lower bounds of the input parameters are given as follows:

$$X_u = [0.001, 0.1, 0.1, 0.1, 60, 25, 0.1, 8000]^T$$

Figure 30. Generic synchronizer performance with gearwheel as a master.



$$\mathbf{X}_u = [0.01, 0.3, 0.35, 0.35, 60, 25, 0.3, 20000]^T$$

In Figure A1(d), Pareto sets points have clear trend with increasing μ_β that shows higher degree of influence of the parameter than other parameters. In (a-c) and (e-h) trends of Pareto sets points are nonuniform because of some floating points with increasing I_r , I_s , r_α , β , α , μ_α and F_{rate} .

As shown in Figure A2, percentage change of I_r , β , μ_β , α and μ_α are higher than percentage change of I_s , r_α and F_{rate} that shows the synchronization performance can be kept in optimized range by allowing the parameters I_r , β , μ_β , α and μ_α to change their values more than the parameters I_s , r_α and F_{rate} . Percentage change of t_{synch} is much less than the percentage change of $\Delta\omega_{s-g}$.

In Figure A3(a-h) t_{synch} and $\Delta\omega_{s-g}$ have opposite trends with increasing I_r , I_s , r_α , μ_β , β , α , μ_α and F_{rate} . In (d) the trends are more clear than in (a-c,e-h). The synchronizer selected at point 1 with eight parameters values is more quicker and less smoother and the synchronizer at point 3 is less quicker and more smoother.

7.2.2. Transmission vibrations

In Figure 31, the generic synchronizer performance is similar as in Figure 26 except the gearwheel (master) has vibrating rotational speed.

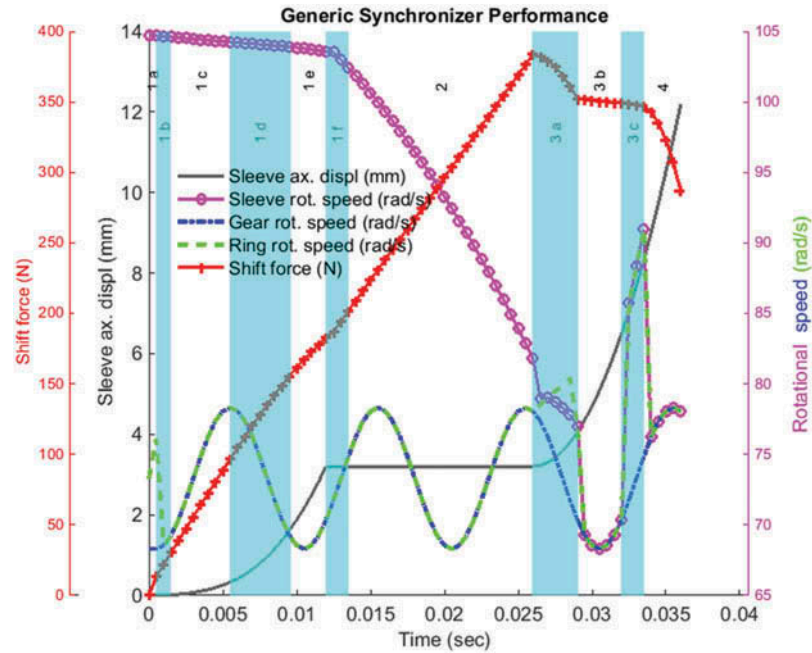
We here study the effect of a periodic variation of the master rotational speed as follows.

$$\dot{\theta}_g^{vib} = \omega_g^{pres} + A_{amp} \sin(2\pi ft + \varphi)$$

In Figure 32, Pareto fronts with transmission vibrations are moving down and right with increasing frequency. At higher synchronization time there is not higher decrease of Pareto fronts in t_{synch} as comparing to Pareto fronts at lower synchronization time while $\Delta\omega_{s-g}$ decreases by reasonable value at all frequencies.

For further cases where gearwheel is considered as a master upper and lower bounds of the input parameters are given below

Figure 31. Generic synchronizer performance with transmission vibrations.

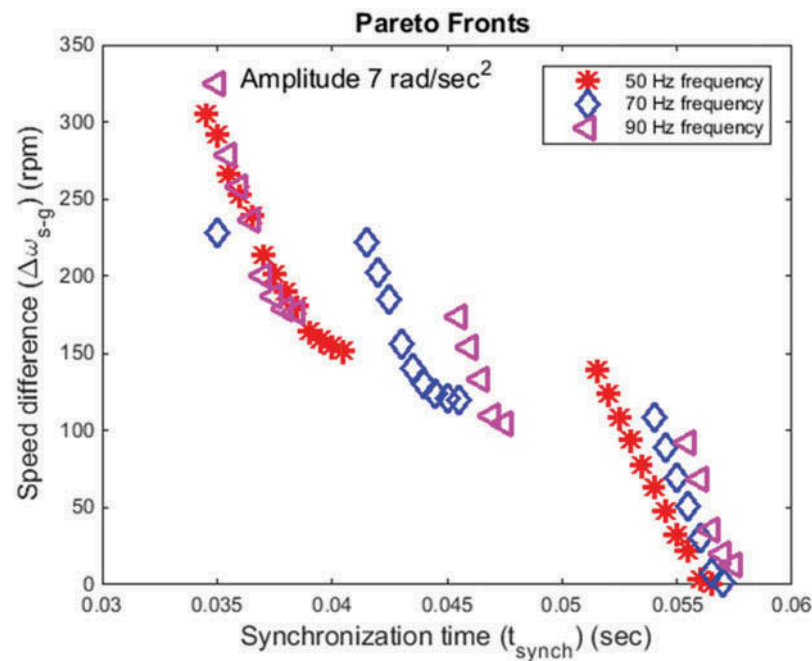


$$X_l = [0.1, 0.25, 0.1, 0.1, 40, 7, 0.1, 8000]^T$$

$$X_u = [0.3, 0.5, 0.2, 0.3, 60, 25, 0.3, 17000]^T$$

In Figure A4 (d), Pareto sets points have significantly an increasing trend with increasing μ_β . There are not clear trends of Pareto sets points in (a,b,c,e,f,g,h) because of floating of points and vibrating nature with increasing $I_r, I_s, r_a, \mu_a, \beta, \alpha$ and F_{rate} .

Figure 32. Pareto fronts at transmission vibrations with varying frequency.



Percentage changes of β , α , μ_α and μ_β are higher and percentage changes of I_r , I_s , r_α and F_{rate} are lower as shown in Figure A5. In the case of transmission vibration with increasing frequency the optimized synchronizer performance can be obtained by allowing β , α , μ_α and μ_β to change their percentage values more than other three parameters. On other hand, I_r , I_s , r_α and F_{rate} can be ignored from the optimization process because of very lower percentage change. Effect of increasing frequency on $\Delta\omega_{s-g}$ is higher than t_{synch} on because percentage change of $\Delta\omega_{s-g}$ is high and percentage change of t_{synch} is less.

In Figure A6(a-c,e-h), Pareto sets points of t_{synch} and $\Delta\omega_{s-g}$ do not have clear trends because of scattering of the points and vibrating nature but in (d) there are clear trends of objectives with increasing μ_β . In the case of vibrations μ_β is the parameter with higher variability.

In Figure 33, Pareto fronts are moving down and right with increasing amplitudes. Increase in t_{synch} is less and increase in $\Delta\omega_{s-g}$ is large.

In Figure A7, I_r and μ_β have highest percentage changes than other parameters which show the synchronizer performance can be kept in optimized range by allowing I_r and μ_β to change their values more than the other parameters. Percentage change of t_{synch} is less with increasing amplitude case than in increasing frequency case but percentage change of $\Delta\omega_{s-g}$ is higher in comparison.

In Figure A8(d), Pareto sets points have significantly an increasing trend with increasing μ_β . In (a-c,e-h) Pareto sets points do not have clear trends with increasing I_r , I_s , r_α , β , α , μ_α and F_{rate} .

7.2.3. Road grade

In Figure 34, the generic synchronizer performance is similar to Figure 30 except the phenomenon that gearwheel (master) continuously loses its rotational speed because of the road grade.

In Figure 35, Pareto fronts stay almost at same level with increasing road grade in the case of gearwheel as a master with upshifting.

Figure 33. Pareto fronts at transmission vibrations with varying amplitude of speed.

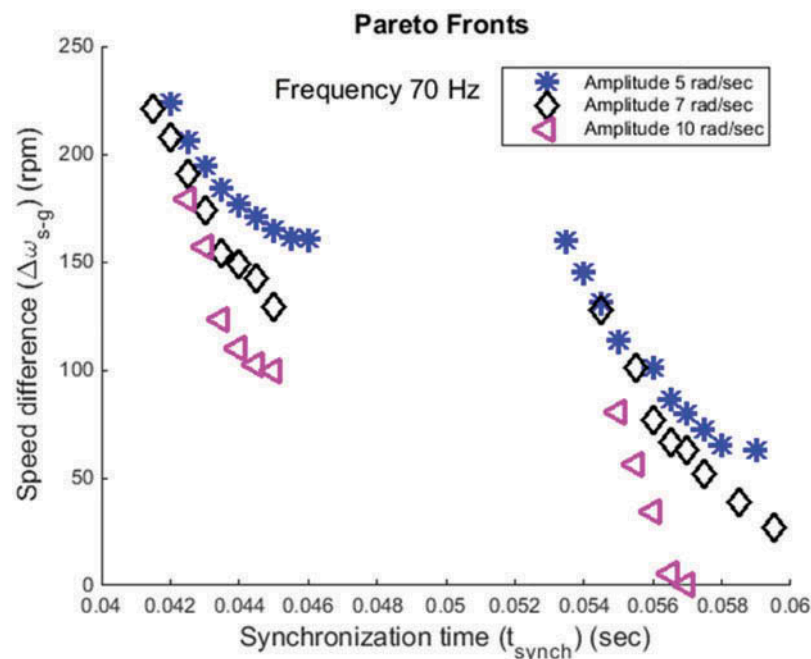
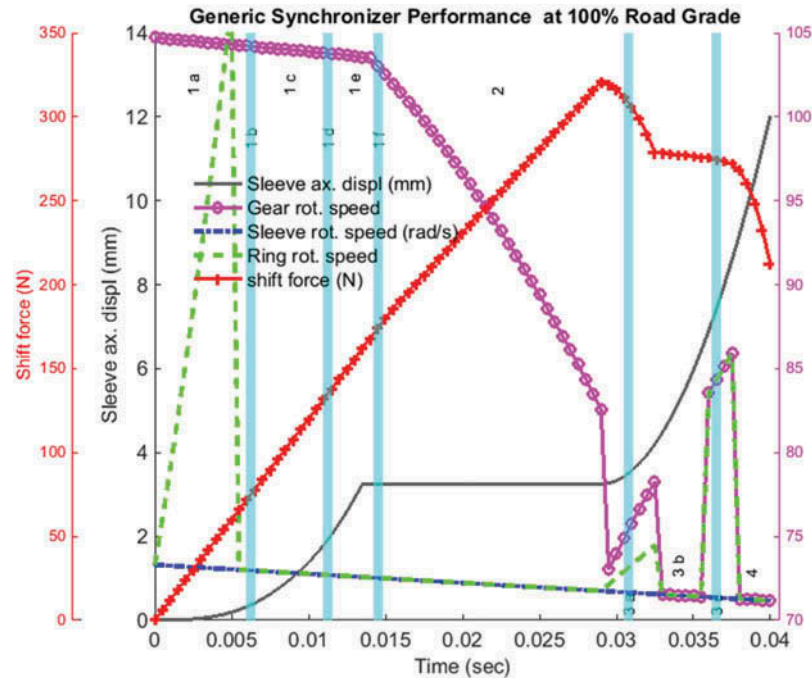


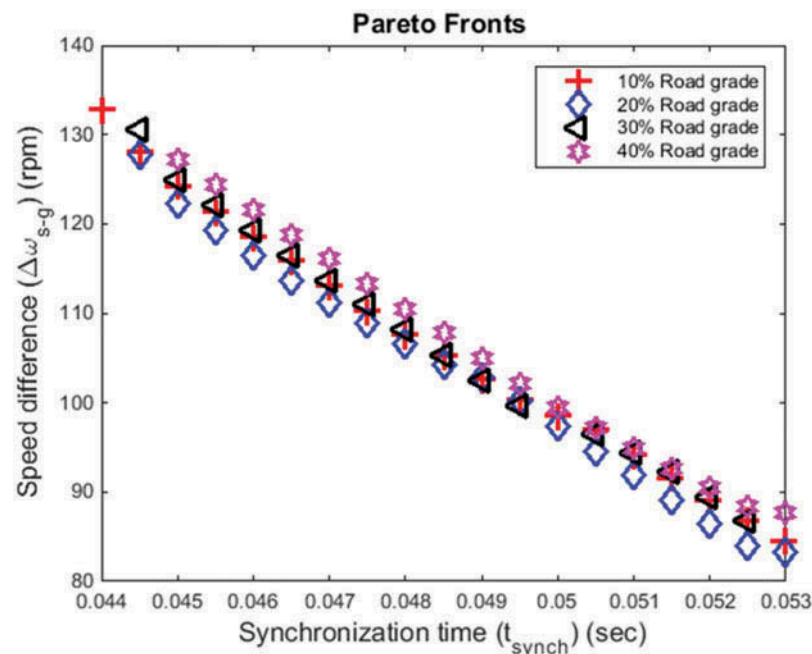
Figure 34. Generic synchronizer performance with road grade.



In Figure A10(a,e), Pareto sets points have trends with increasing I_r and β and in (b-d,f-h) Pareto sets points have no significant trends with increasing I_s , r_a , μ_β , α , μ_a , and F_{rate} . Variability of the parameters I_r and β are higher than the other parameters in the optimized range of Pareto front.

As shown in Figure A11 I_r and μ_β is the most important parameter to keep the synchronizer performance in optimized range because of higher percentage change. The percentage change of $\Delta\omega_{s-g}$ in Figure A11 is higher but not important because $\Delta\omega_{s-g}$ in Figure 35 changes from 80 to 130 rpm.

Figure 35. Pareto fronts with increasing road grade.



In Figure A12(b,c,f,g), most of points of I_s , r_α , α and μ_α are along the vertical line that indicates I_s , r_α , α and μ_α can be ignored from the input parameters for optimization of the synchronization.

7.3. Sleeve and gearwheel as slaves

There can also be practical cases when both sleeve and gearwheel are slaves (such as the split gear synchronizer that is not connected with the wheels). It is found in the previous case where the sleeve is considered as a slave that the synchronization time is 0.09 sec as shown in Figure 4 but in the case where the gearwheel is considered as a slave the synchronization time is 0.04 s as shown in Figure 30. The decrement in time is more than 50%. So it is quite curious to study the case where both the sleeve and the gearwheel should be considered as slaves.

7.3.1. Nominal case

The generic synchronizer performance in Figure 36 is similar to Figure 4 with exception of shorter synchronization time when the sleeve and the gearwheel are slaves.

For the case where sleeve and gearwheel are considered as slaves upper and lower bounds of the input parameters are given as follows:

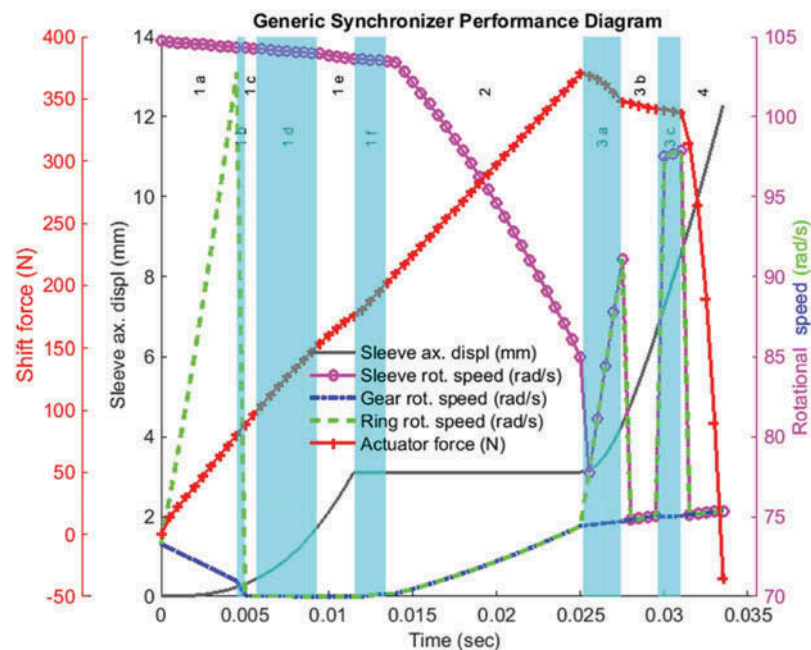
$$X_l = [0.001, 0.1, 0.1, 0.1, 40, 7, 0.1, 8000]^T$$

$$X_u = [0.01, 0.3, 0.35, 0.35, 60, 25, 0.3, 20000]^T$$

In Figure A13(a,d,f,h), Pareto sets points have trends with increasing I_r , μ_β , α and F_{rote} and in (b,c, e,g) Pareto sets points do not have significant trends with increasing I_s , r_α , β and μ_α .

In Figure A14, percentage changes of I_r , I_s , μ_β and α are higher than other parameters. The percentage change of $\Delta\omega_{s-g}$ is higher but not important as comparing to other cases because $\Delta\omega_{s-g}$ changes from 1 rpm to 140 rpm. The percentage change of t_{synch} is also less than other cases and percentage changes of all parameters are less than percentage changes in other cases where one of the rotating body considered as a master.

Figure 36. The generic synchronizer performance with sleeve and gearwheel as slaves.



7.3.2. Transmission vibrations

Before engaging to next gear, the sleeve must be disengaged from the previous gear. There are chances of producing the vibrations during disengagement and also because of the disengagement of the clutch. These vibrations will also affect the gear-shifting process. So the effect of vibrations is studied when both the sleeve and the gear are considered as slave.

In Figure 37, the generic synchronizer performance is similar to Figure 4 with an addition of transmission vibrations for rotational speed of the sleeve and the gearwheel.

In Figure A16, Pareto fronts decrease with increasing frequency. At higher frequencies Pareto fronts decrease more than at lower frequencies.

For further cases where the sleeve and the gearwheel are considered as slaves, moment of inertia of sleeve is taken into the vector input parameter ($X = [I_r, I_s, r_a, \mu_\beta, \beta, \alpha, \mu_\alpha, F_{rate}]^T$). Upper and lower bounds of the input parameters in the Pareto optimization problem are given below

$$X_l = [0.1, 0.25, 0.1, 0.1, 40, 7, 0.1, 8000]^T, X_u = [0.3, 0.5, 0.2, 0.3, 60, 25, 0.3, 17000]^T$$

In Figure A17(e, f, h), Pareto sets points have clear trends with increasing β, α and F_{rate} whereas in (a-d, g) Pareto sets points do not have clear trends with increasing $I_r, r_a, I_g, \mu_\alpha$ and μ_β .

In Figure A18, I_s, β, μ_β and F_{rate} have percentage changes are 37, 13, 18, and 27, respectively. Others 4 parameters have very small percentage changes therefore those parameters can be ignored from the input parameters for the optimization of the generic synchronization process. Percentage change of $\Delta\omega_{s-g}$ is higher than change of t_{synch} .

In Figure A19(a-d, g), Pareto sets points of $\Delta\omega_{s-g}$ and t_{synch} do not have significant trends with increasing $I_r, r_a, I_s, \mu_\alpha$ and μ_β . Pareto sets points of $\Delta\omega_{s-g}$ and t_{synch} have clear trends with increasing β, α and F_{rate} .

Pareto fronts stay almost at same level with increasing amplitude as shown in Figure A20. t_{synch} and $\Delta\omega_{s-g}$ do not vary with Pareto fronts.

Figure 37. The generic synchronizer performance with transmission vibration.

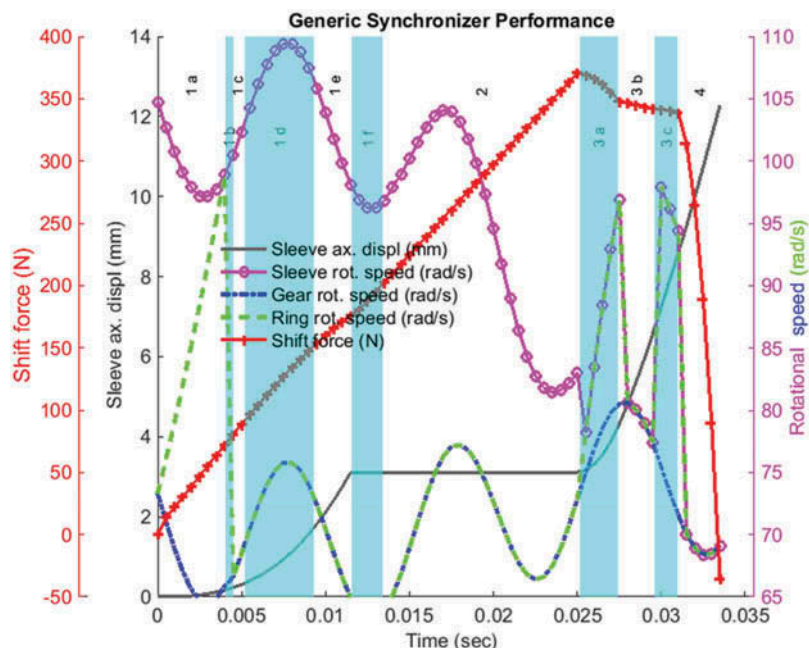


Table 5. Parameters with higher degree of influence in eight cases

Sleeve as a master	Gear as a master	Both slave
Nominal	Nominal	Nominal
$\mu_\beta, \beta, \alpha, \mu_\alpha$ and F_{rate}	$I_r, \mu_\beta, \beta, \alpha$ and μ_α	I_r, I_s, μ_β and α
Vibrations	Vibrations	Vibrations
$I_r, \mu_\beta, \alpha, \mu_\alpha$ and F_{rate}	$I_r, \mu_\beta, \beta, \mu_\alpha$ and α	I_s, μ_β, β and F_{rate}
Road grade	Road grade	
$r_\alpha, \mu_\beta, \beta, \alpha, \mu_\alpha$ and F_{rate}	I_r, μ_β and β	

In Figure A21(e), Pareto sets points have trends with increasing β while in (a-b,f-h) Pareto sets points do not have clear trends with increasing $I_r, I_s, r_\alpha, \alpha, \mu_\beta, \mu_\alpha$ and F_{rate} .

In Figure A22, I_s, μ_β, β and F_{rate} have highest percentage change but in Figure A19(a) I_s and μ_β have no trends. So I_s, μ_β, β and F_{rate} are the parameters which can keep the synchronizer performance in optimized range than the other parameters.

In Figure A23(e), Pareto sets points of $\Delta\omega_{s-g}$ and t_{synch} have trends with increasing β while the Pareto sets points do not have significant trends with increasing $I_r, I_s, \alpha, \mu_\alpha, r_\alpha, \mu_\beta$ and F_{rate} .

Most influencing parameters in each case are given in Table 5.

As shown in Table 5, $F_{rate}, \beta, \alpha, \mu_\alpha$ and μ_β are the most influencing parameters in most of the cases. For example in a case where gear is master at nominal condition $I_r, \beta, \alpha, \mu_\alpha$ and μ_β are the most influencing parameters whereas in the case where sleeve is master at road grade condition $r_\alpha, \beta, \mu_\beta, \mu_\alpha$ and F_{rate} are most influencing parameters. While some of the parameters have very less influence in few cases for example r_α has very less influence in the case of vibrating sleeve/gear as a master. When both the sleeve and the gear are slave, the gear-shifting process will not have any effect of the road grade. So the road grade is not studied in the case where both the sleeve and the gear are considered as slave.

8. Conclusions and outlook

The most important outcome of the study is the identification of degree of influence of the parameters under different scenarios. The following eight parameters of the generic synchronizer are considered: cone angle, cone coefficient of friction, applied shift force, blocker angle, blocker coefficient of friction, cone radius, gear moment of inertia, and ring moment of inertia. The developed computational model of a generic synchronizer based on CLF is used to study the gear-shifting process. In local sensitivity analysis, effect of each parameter is analyzed on the objective functions. It is found that all eight parameters have reasonable effect on the objective functions. In the optimization process, eight parameters are considered as input parameters. Eight cases are studied under different scenarios of master/slave and different operating conditions of road grade, vibrations, and nominal. To find the degree of influence of the parameters from the results of optimization three different approaches are used; Pareto sets points are plotted along the Pareto front, percentage change of the parameters are calculated within the limits of variation of the parameters values and objective functions are plotted along the parameters. It is found that all eight parameters do not have same degree of influence on the objective functions. Some parameters have very high degree of influence and some parameters have very low degree of influence. The parameters with lowest degree of influence can be ignored while deciding about the optimized performance of the generic synchronizer. The parameters which cannot be ignored are given in Table 5.

It is suggested for future work to verify the developed synchronizer model and relevant results with industrial simulation tool. It is also proposed to implement the friction model developed in Häggström et al. (2016).

Definitions/abbreviations

θ_{r-s}	Displacement difference between ring and sleeve
S_{eng}	Engaging teeth axial length
θ_{g-s}	Displacement difference between gear and sleeve
x_{eng}	Full engaging length
T_I	Index torque

Funding

This work was supported by the Swedish Agency for Innovation Systems, VINNOVA, project No. 2012-04619.

Author details

Muhammad Irfan¹
 E-mail: irfan.muhammad@chalmers.se
 ORCID ID: <http://orcid.org/0000-0002-3569-3383>
 Viktor Berbyuk¹
 E-mail: viktor.berbyuk@chalmers.se
 ORCID ID: <http://orcid.org/0000-0002-8862-1148>
 Håkan Johansson¹
 E-mail: hakan.johansson@chalmers.se
 ORCID ID: <http://orcid.org/0000-0002-7207-8486>

¹ Division of Dynamics, Department of Mechanics and Maritime Sciences, Chalmers University of Technology, Gothenburg, Sweden.

Citation information

Cite this article as: Performance improvement of a transmission synchronizer via sensitivity analysis and Pareto optimization, Muhammad Irfan, Viktor Berbyuk & Håkan Johansson, *Cogent Engineering* (2018), 5: 1471768.

Cover Image

Source:

References

- Abel, A., Schreiber, U., & Schindler, J. (2006, April 3-6). Engine and gearbox modeling and simulation for improving the shifting behavior of powertrains with manual or automated transmission. SAE Technical Paper 2006-01-1641, 2006, <https://doi.org/10.4271/2006-01-1641>.
- Berbyuk, V. (2015, August 2-5). Towards pareto optimization of performance of a generic synchronizer of transmission systems. In *proceedings of IDETC/CIE 2015 ASME conference*. Boston, USA (paper DETC 2015-46773). doi:10.1115/DETC2015-46773.
- Gong, Z., Zhang, W., Chen, G., & Wang, W. (2008). Analyses and evaluation on synchronizer of manual transmission. *IEEE Pacific-Asia workshop on computational intelligence and industrial application*. Wuhan, China.
- Gustavsson, A. (2009). *Development and analysis of synchronization process control algorithms in a dual clutch transmission*. Linköping, Sweden: Department of Electrical Engineering Linköpings universitet.
- Häggström, D. (2016). *On synchronization of heavy truck transmissions* (Licentiate thesis). Stockholm, Sweden: Department of Machine Design KTH Royal Institute of Technology SE-100 44.
- Häggström, D., & Nordlander, M. (2011). *Development of a program for calculating gearbox synchronization* (Master thesis). Södertälje, Luleå: Department of Engineering Sciences and Mathematics, Luleå University of Technology.
- Häggström, D., Nyman, P., Sellgren, U., & Björklund, S. (2016). Predicting friction in synchronizer systems. *Tribology International*, 97, 89–96. doi:10.1016/j.triboint.2015.12.038
- Häggström, D., Sellgren, U., Stenström, W., & Björklund, S. (2015, August 2–5). A verified and validated model for simulation-driven design of heavy duty truck synchronizers. In *ASME 2015 power transmission and gearing conference; 23rd reliability, stress analysis, and failure prevention conference*. Boston, Massachusetts.
- Hoshino, H. (1999, March 1-4). *Analysis on synchronization mechanism of transmission*. Detroit, Michigan: International Congress and Exposition.
- Irfan, M., Berbyuk, V., & Johansson, H. (2015a). *Constrained Lagrangian formulation for modelling and analysis of transmission synchronizers*. Gothenburg: Department of Applied Mechanics Chalmers University of Technology.
- Irfan, M., Berbyuk, V., & Johansson, H. (2015b, September 7-10). Modelling of heavy vehicle transmission synchronizer using constrained Lagrangian formalism. In *International conference on engineering vibration*. Ljubljana, Slovenia.
- Irfan, M., Berbyuk, V., & Johansson, H. (2016). Dynamics and Pareto optimization of a generic synchronizer mechanism. *Rotating Machinery, Proceedings of the 34th IMAC, A Conference and Exposition on Structural Dynamics*, 8, 417–425. doi:10.1007/978-3-319-30084-9_38.
- Kelly, D., & Kent, C. (2000, June 12-15). Gear shift quality improvement in manual transmissions using dynamic modelling. *FISITA world automotive congress*. Seoul, Korea.
- Liu, Y., & Tseng, C. (2007). Simulation and analysis of synchronisation and engagement on manual transmission gearbox. *International Journal Vehicle Design*, 43. doi:10.1504/IJVD.2007.012304
- Lovas, L. (2004). *Etude des relations entre le comportement et la fabrication des synchronisateurs des synchronisateurs des* (PhD Thesis). Lyon: National Institute of Applied Sciences.
- Razzacki, S. T., & Hottenstein, J. E. (2007). Synchronizer design and development for dual clutch transmission. *SAE Technical Paper*, 10. doi:10.4271/2007-01-0114
- Sahlholm, P., & Johansson, K. H. (2010, November). Road grade estimation for look-ahead vehicle control

using multiple measurement runs. *Control Engineering Practice*, 18(11), 1328–1341.
 doi:10.1016/j.conengprac.2009.09.007

Sandooja, A. (2012). Double synchronizer to amplify the synchronizer capacity. *SAE Technical Paper Series*.
 doi:10.4271/2012-01-2003,

Sharma, M. K., & Salva, J. (2012). Shift system inertia mass optimization techniques to minimize double bump for manual transmission. *SAE technical paper 2012-01-1999*, 2012, doi:10.4271/2012-01-1999.

Stenvall, H. (2010). *Driving resistance analysis of long haulage trucks at Volvo*. Göteborg, Sweden: 2010:18 Division of Vehicle engineering & autonomous systems department of applied mechanics Chalmers University of Technology.

Yuming, G. (2011, November 3–5). Discuss designing method of transmission synchronizer. In *International conference on advanced technology of design and manufacture (ATDM2011)*. Changzhou, China.

Appendix

Gearwheel as a slave

Optimization results in the case where the gearwheel is considered as a slave are shown in Figure A1–12.

Figure A1: Variation of Pareto sets points of parameters with Pareto front.

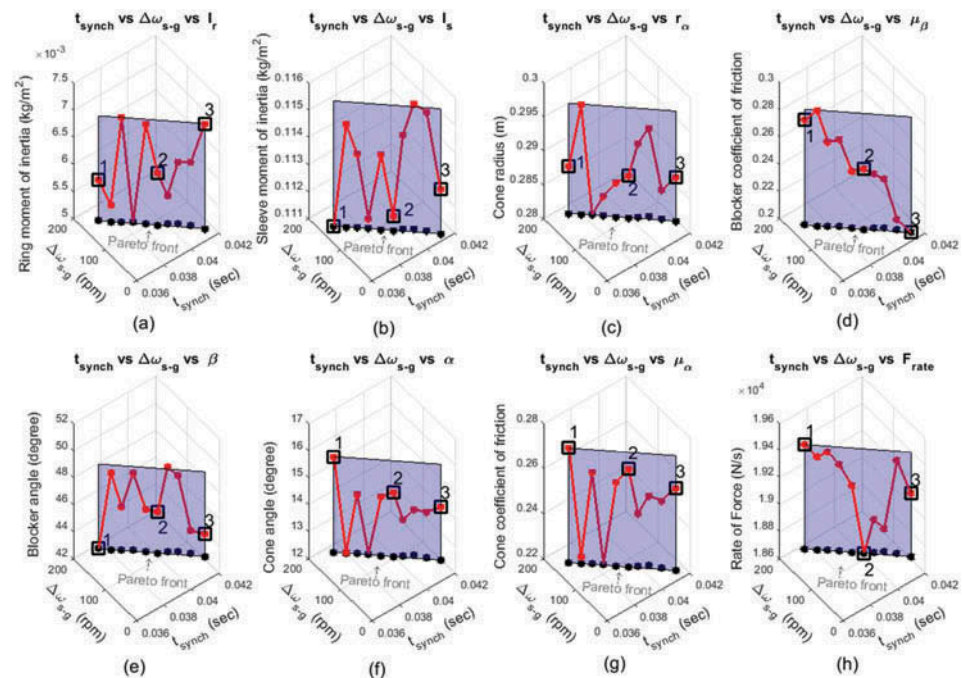


Figure A2: Normalized percentage change of input parameters and objectives.

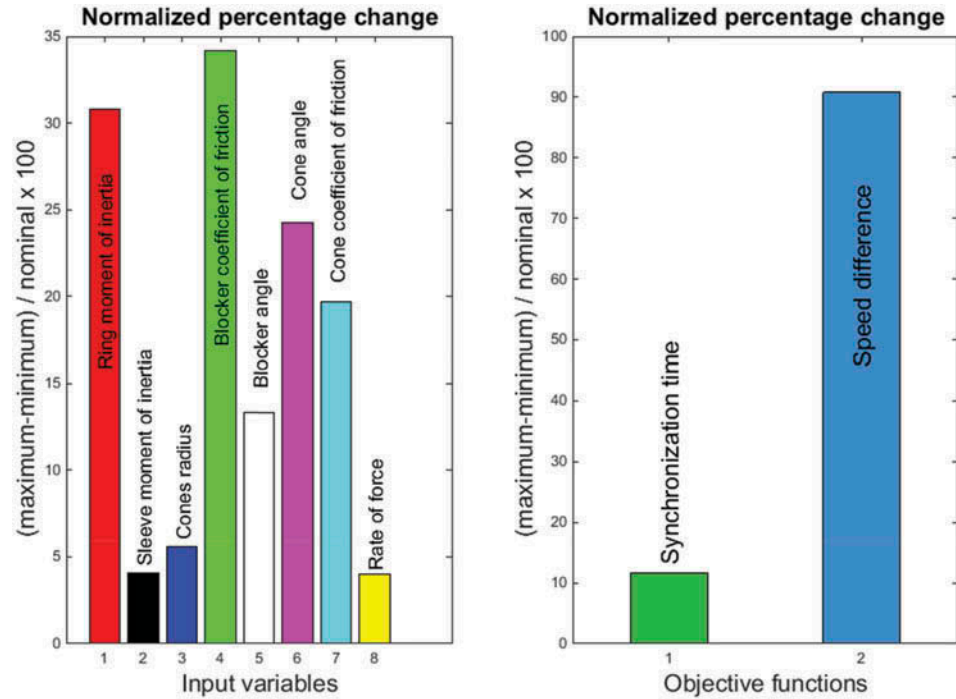


Figure A3: Parameters with objectives in optimal range.

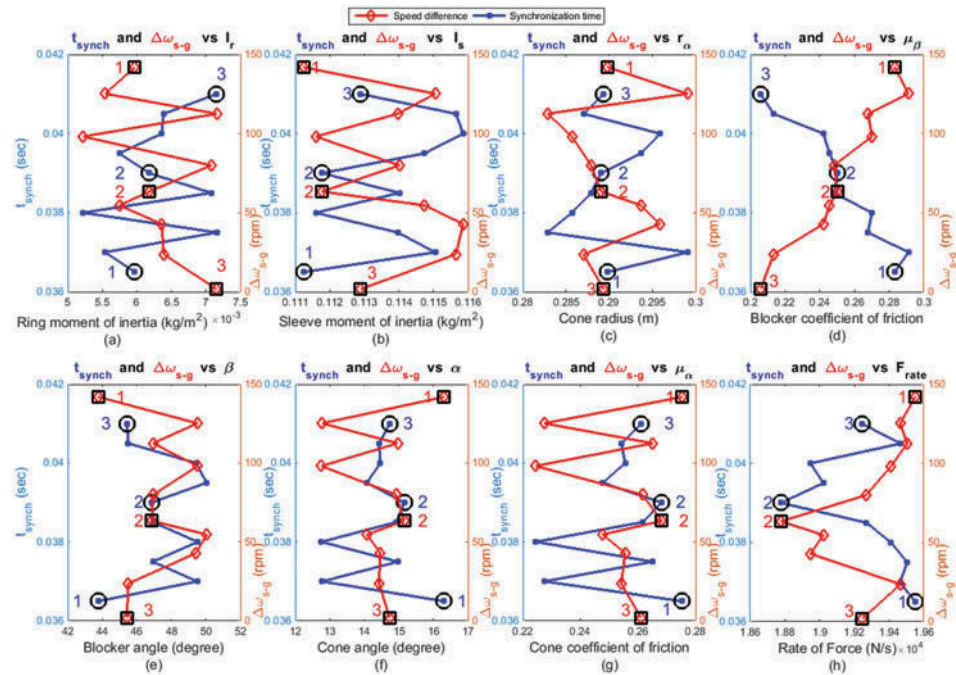


Figure A4: Pareto sets points of eight parameters at vibrations with 70 Hz frequency.

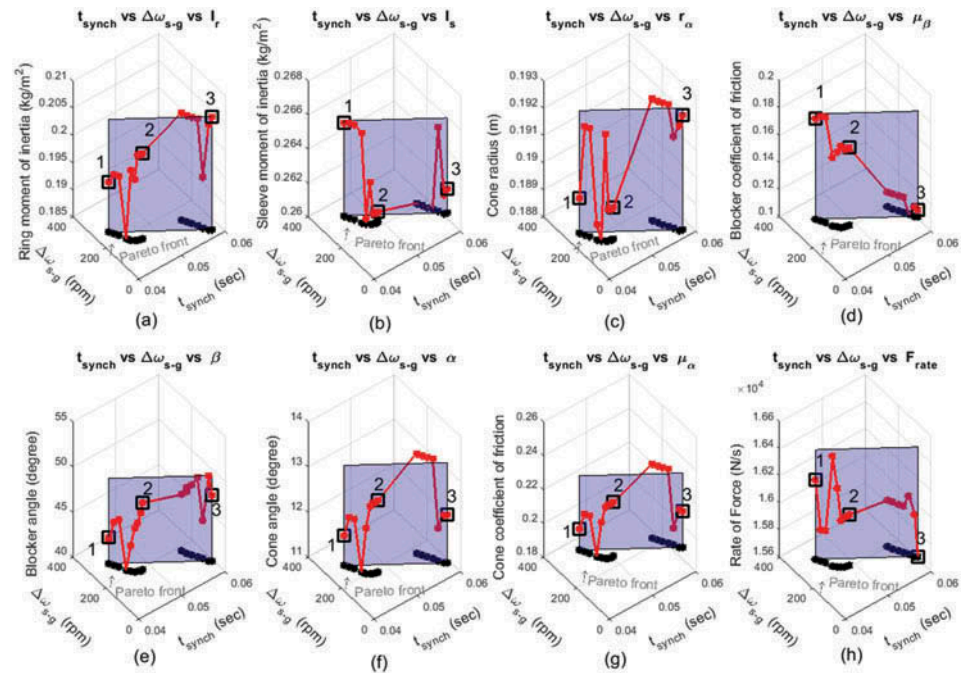


Figure A5: Normalized percentage change of parameters and objectives.

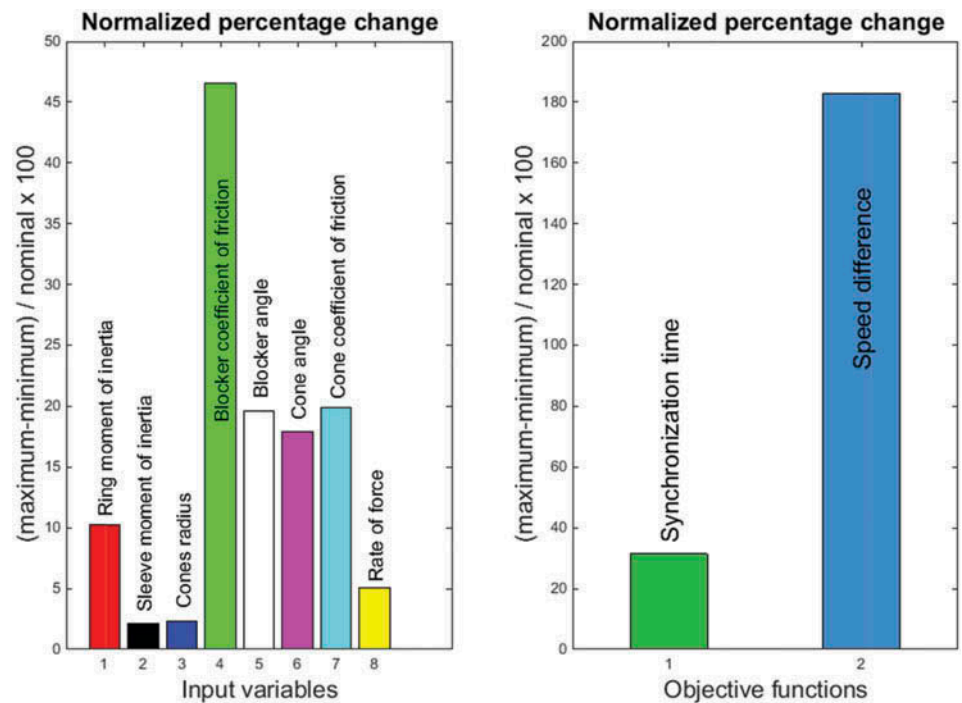


Figure A6: Variation of objectives with parameters at vibration of 70-Hz frequency.

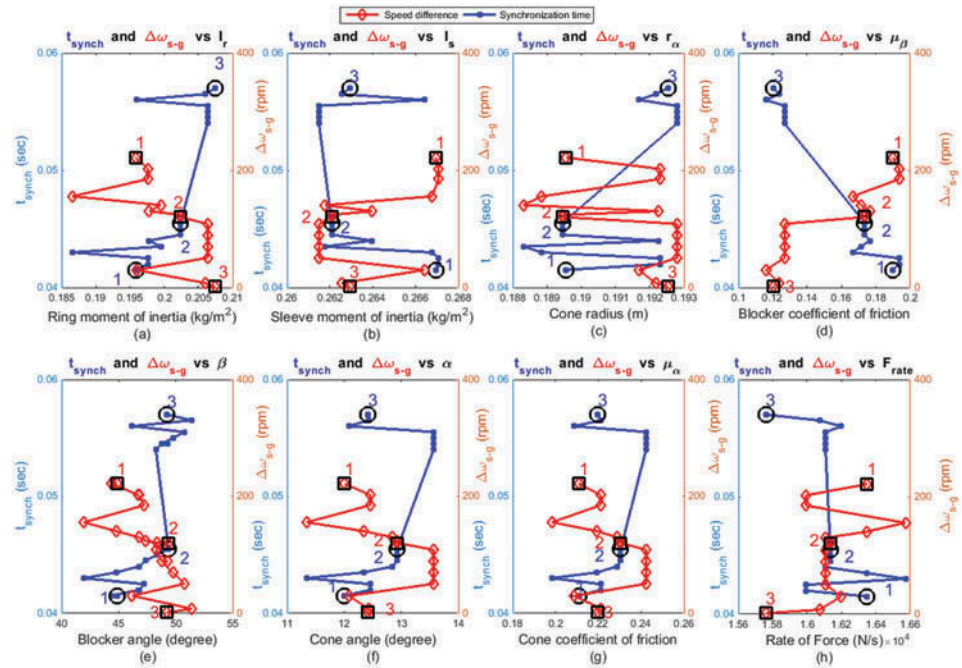


Figure A7: Percentage change of objectives and parameters.

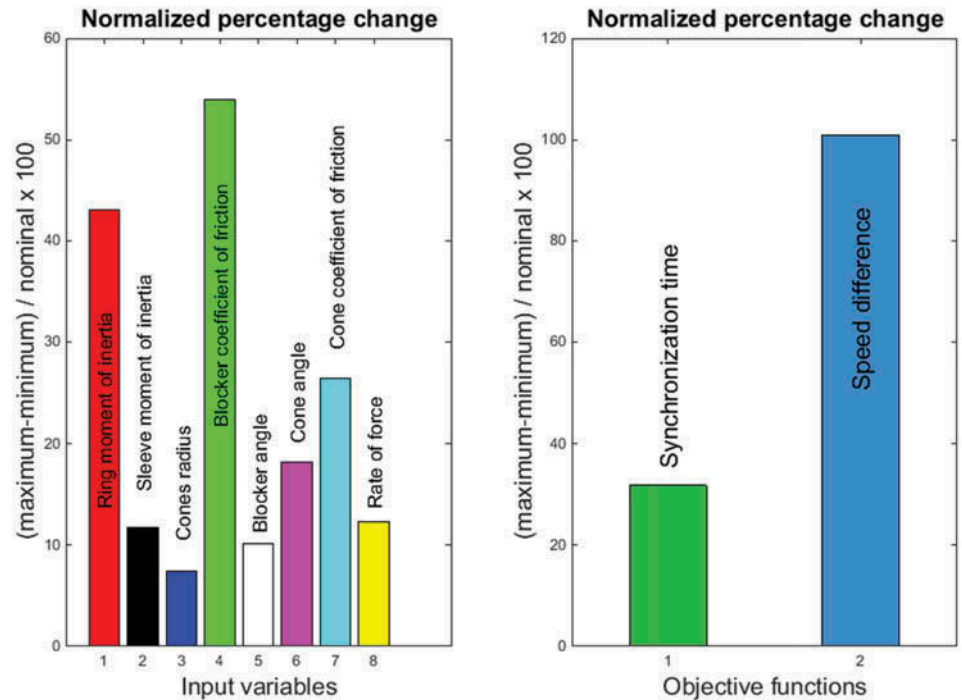


Figure A8: Variation of Pareto sets points of parameters with Pareto front at vibrations with 5 rad/sec amplitude.

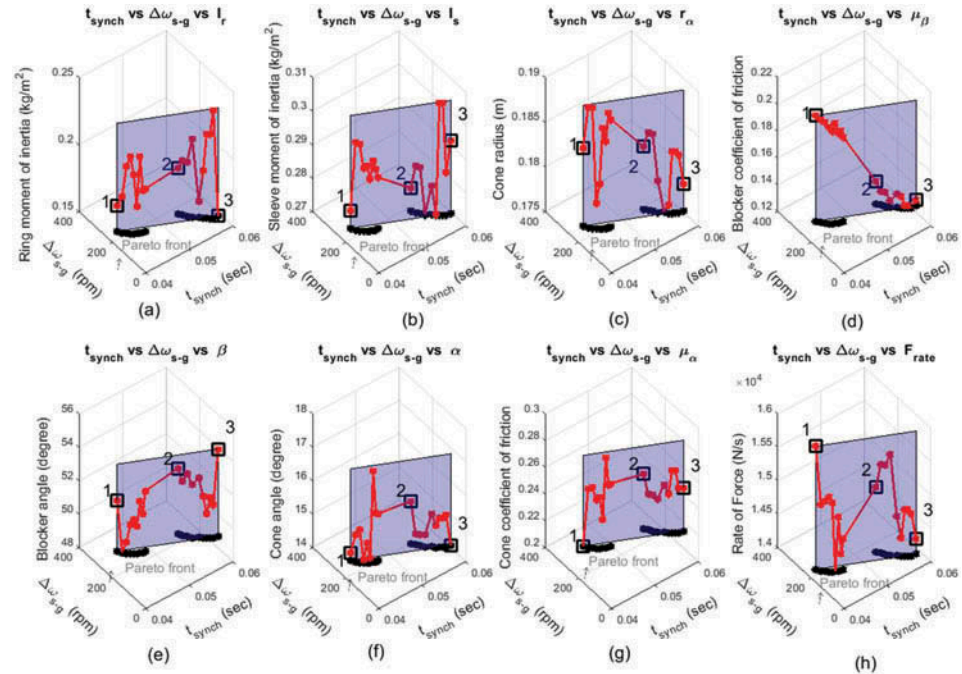


Figure A9: Variation of parameters with objectives at vibrations with 5 rad/sec amplitude.

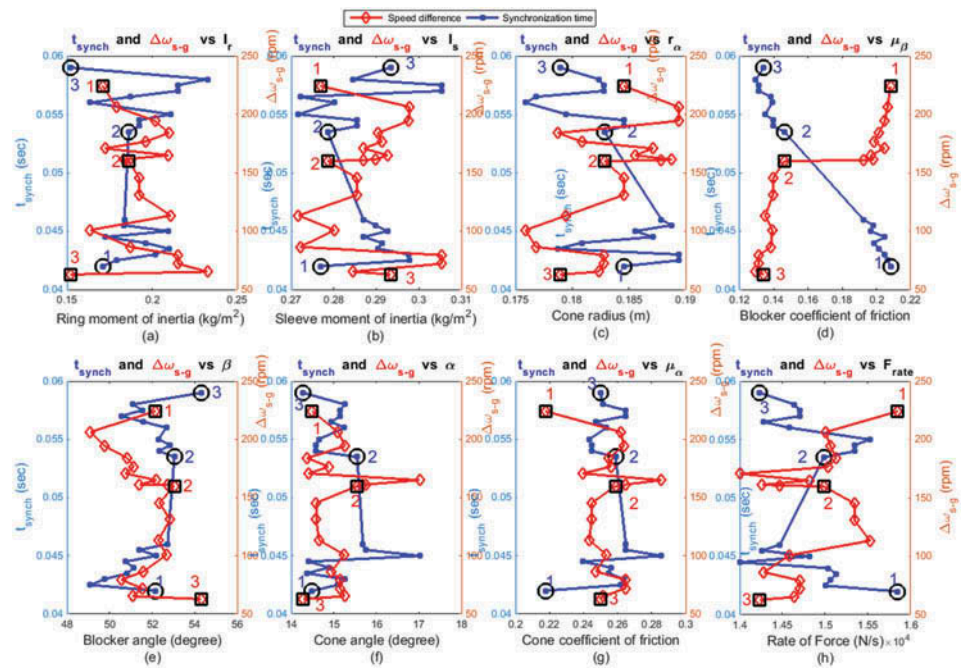


Figure A10: Variation of Pareto sets points of parameters with Pareto front at 10% road grade.

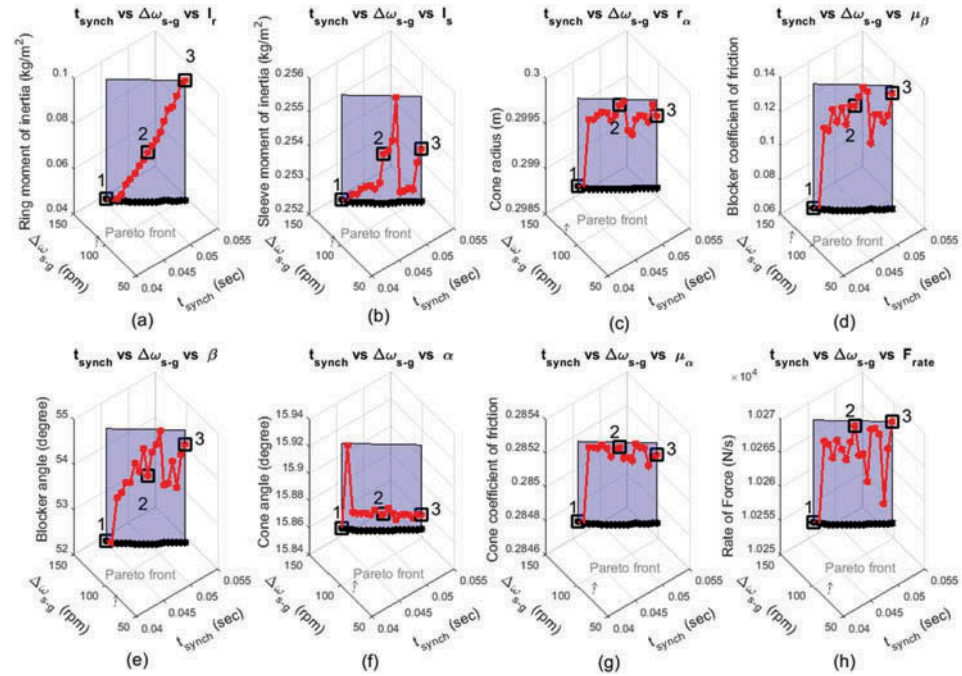


Figure A11: Percentage change of parameters and objectives.

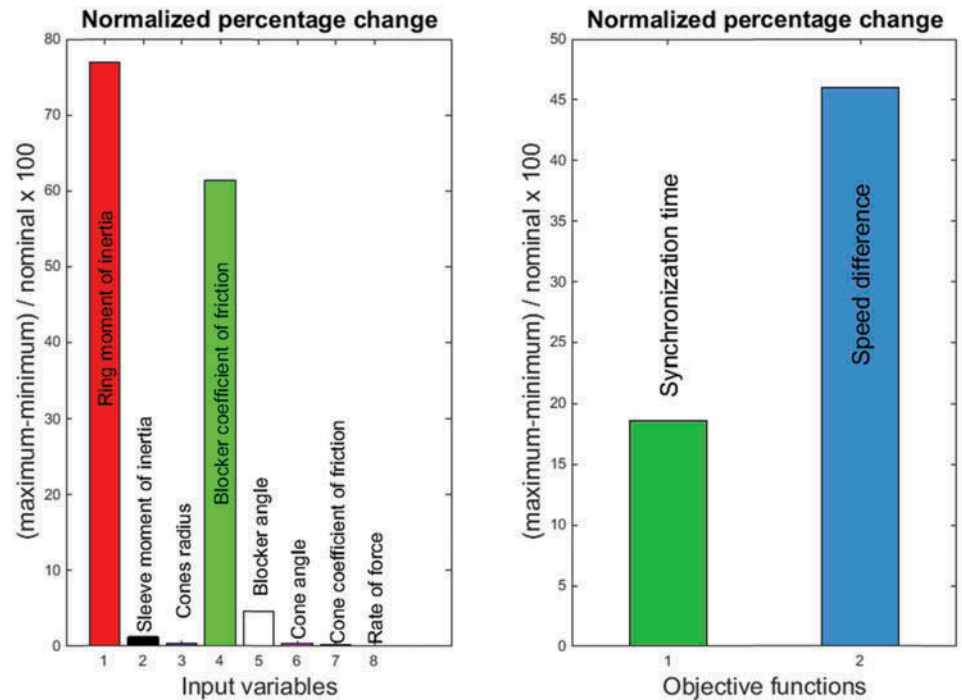
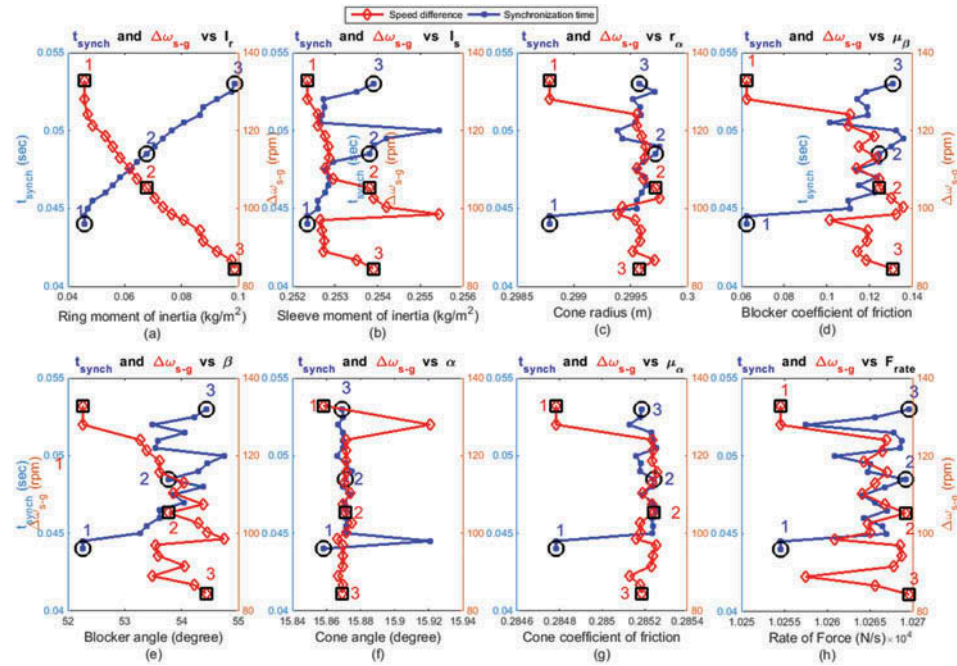


Figure A12: Variation of objectives with parameters at 10% road grade.



Sleeve and Gearwheel as a slaves

Optimization results in the case where the sleeve and the gearwheel are considered as slaves are shown in Figures A13–21.

Figure A13: Variation of Pareto sets points of parameters with Pareto front.

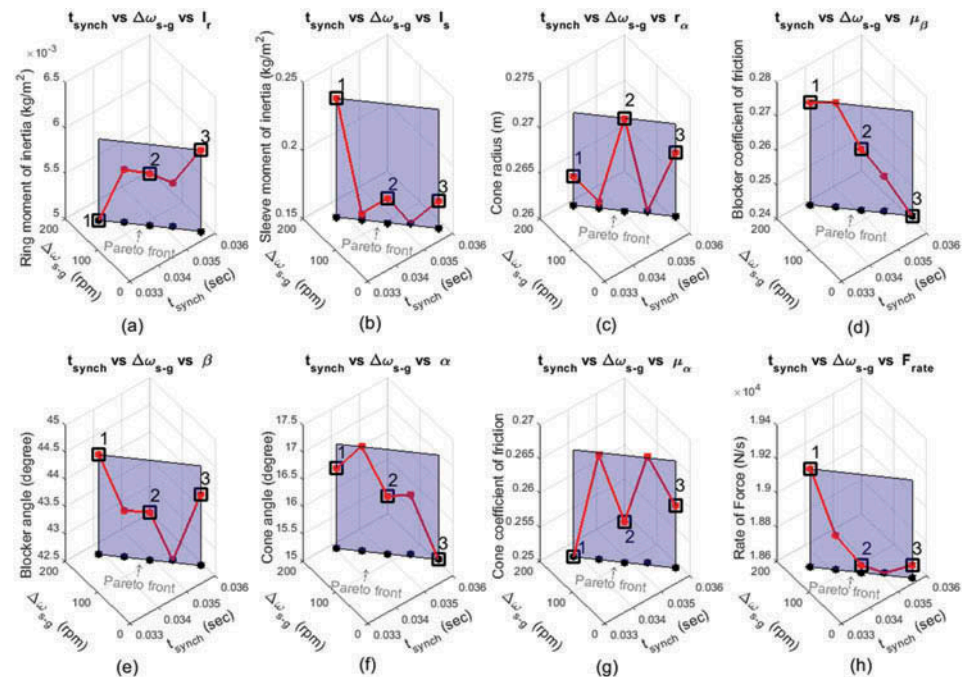


Figure A14: Normalized percentage change of objectives and parameters.

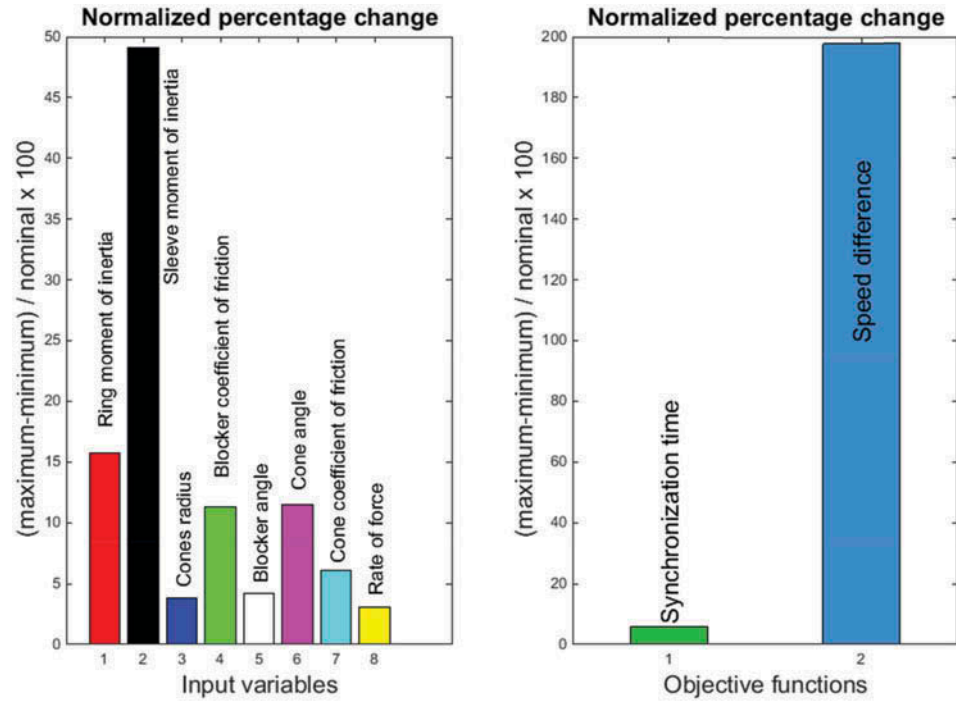


Figure A15: Variation of objectives with parameters.

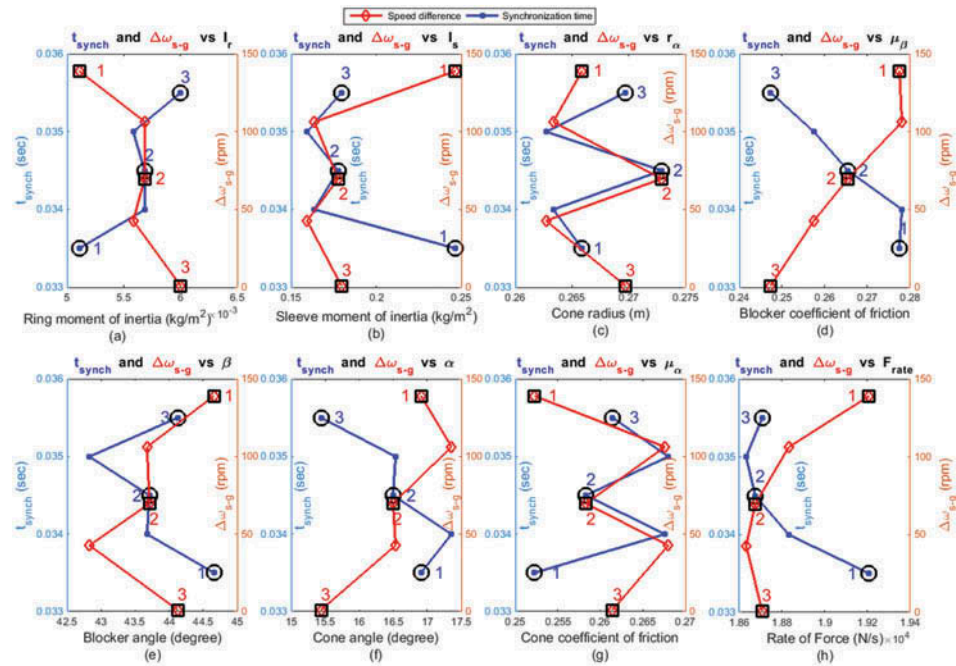


Figure A16: Pareto fronts with increasing frequency.

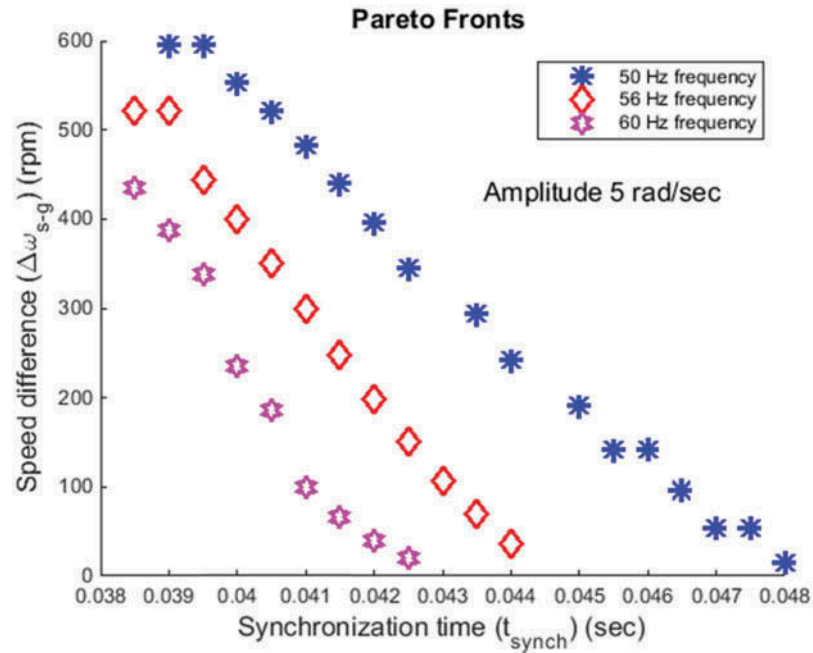


Figure A17: Variation of Pareto sets points of parameters with Pareto front at 50 Hz frequency.

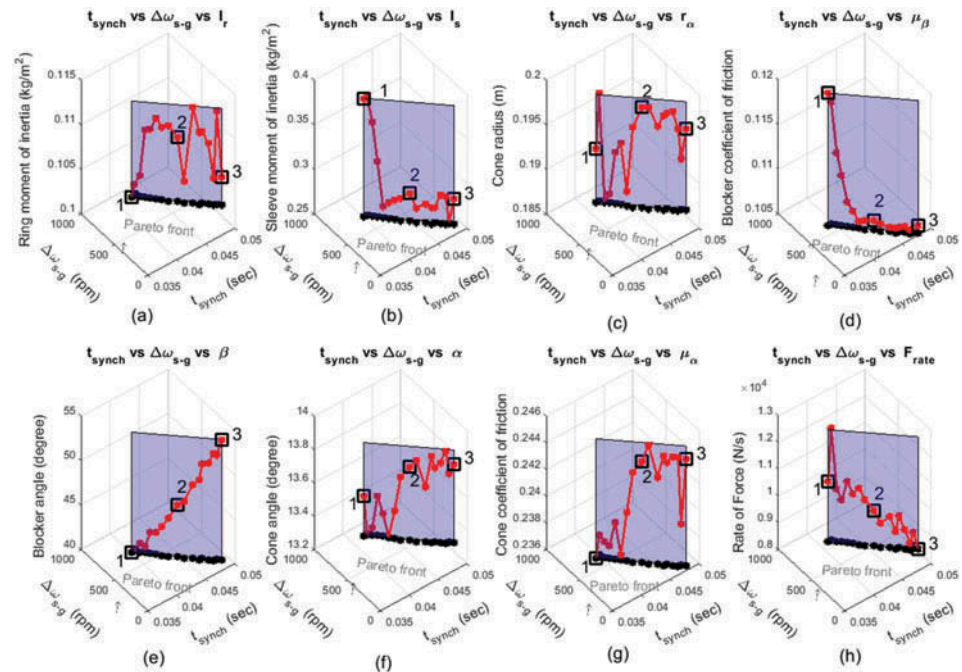


Figure A18: Variation of objectives with parameters at 50 Hz frequency.

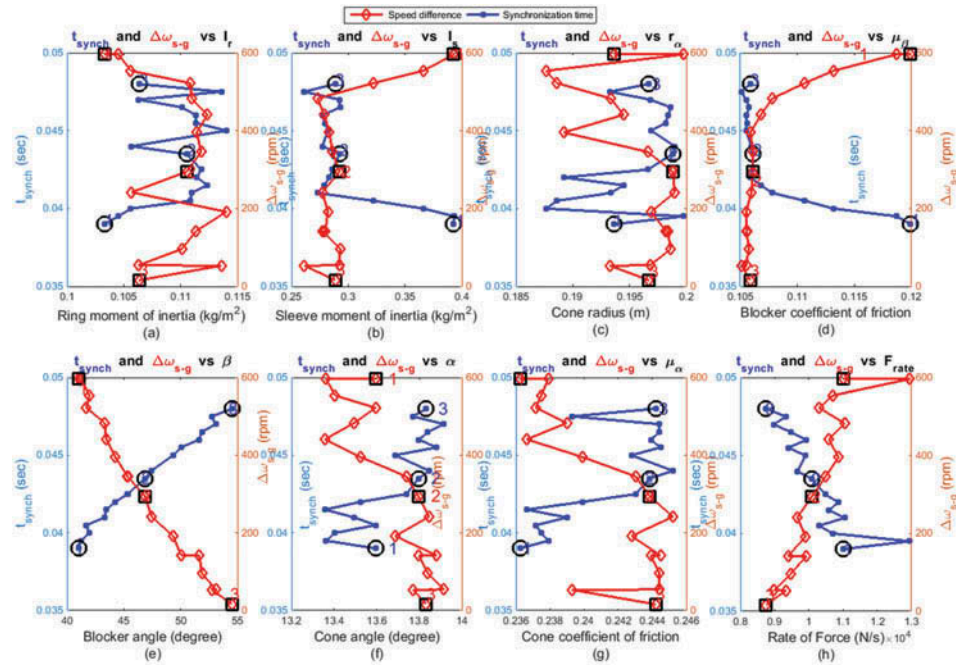


Figure A19: Normalized percentage changes of parameters and objectives.

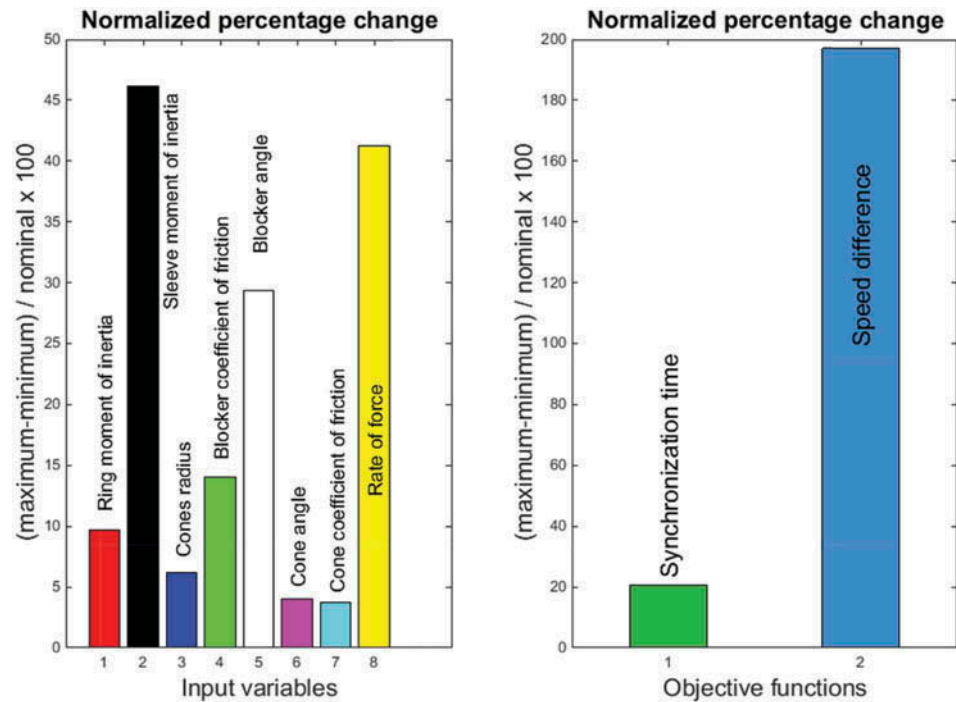


Figure A20: Pareto fronts with increasing amplitude of speed.

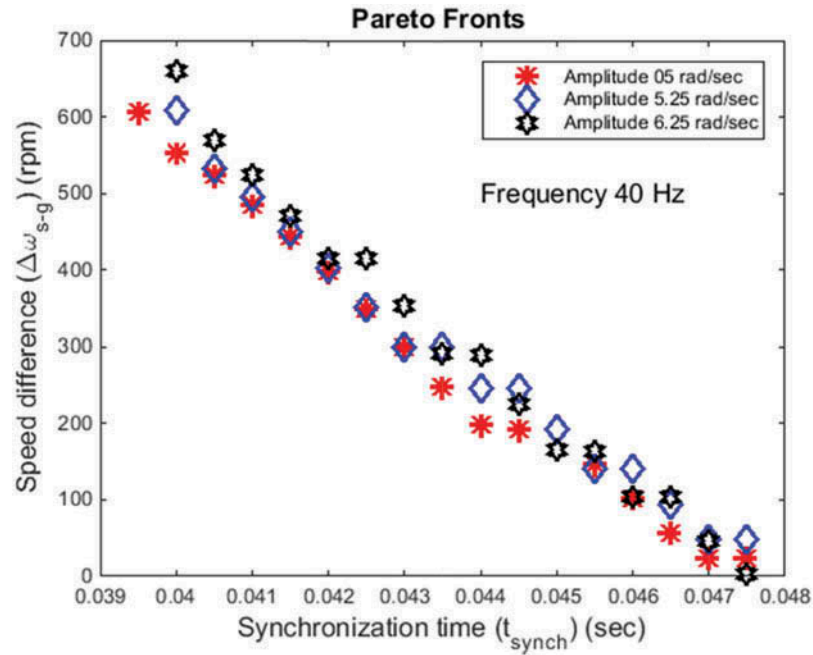


Figure A21: Variation of Pareto sets points of parameters with Pareto front at 5 rad/sec amplitude.

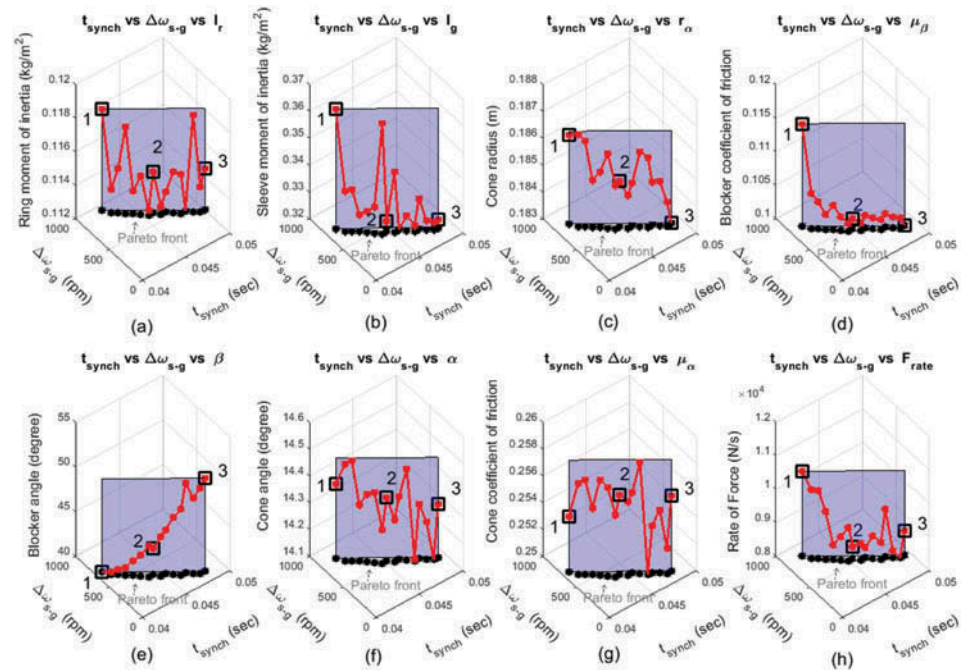


Figure A22: Normalized percentage changes of parameters and objectives.

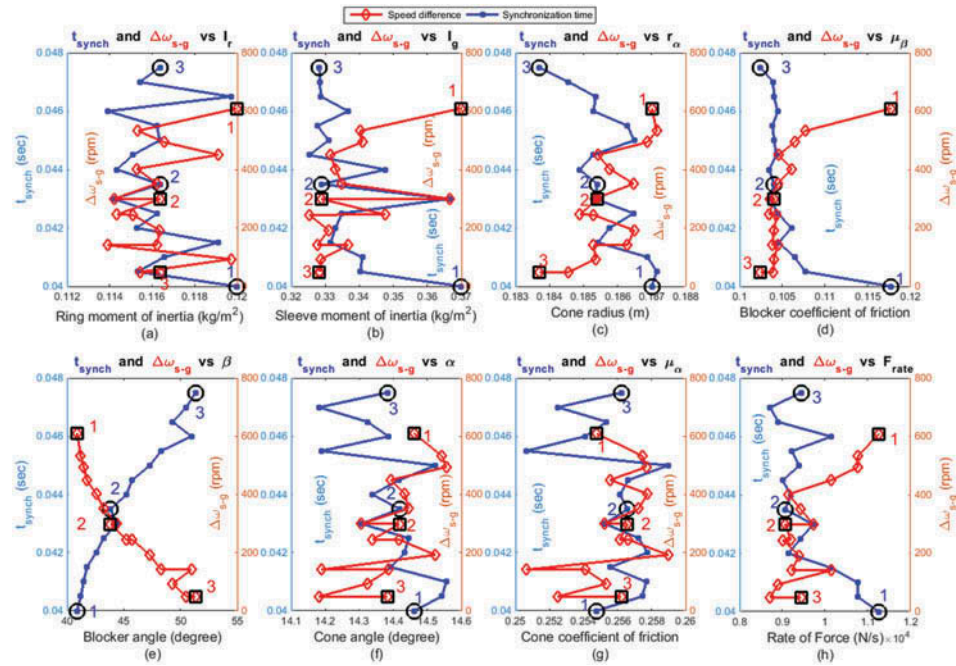
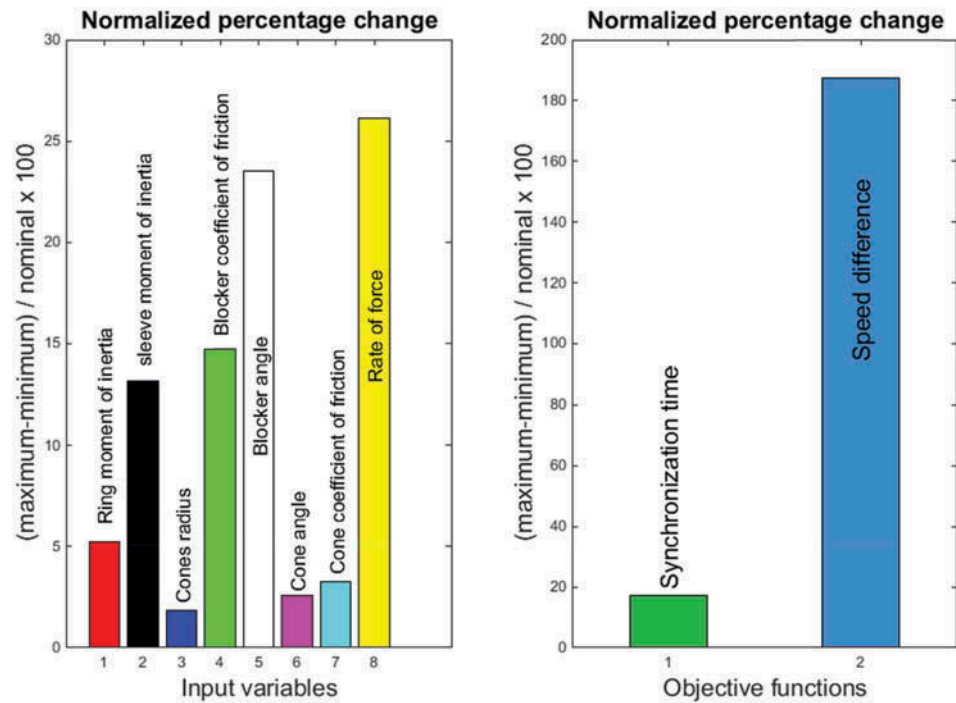


Figure A23: Variation of objectives with parameters at 5 rad/s amplitude.





© 2018 The Author(s). This open access article is distributed under a Creative Commons Attribution (CC-BY) 4.0 license.

You are free to:

Share — copy and redistribute the material in any medium or format.

Adapt — remix, transform, and build upon the material for any purpose, even commercially.

The licensor cannot revoke these freedoms as long as you follow the license terms.

Under the following terms:

Attribution — You must give appropriate credit, provide a link to the license, and indicate if changes were made.

You may do so in any reasonable manner, but not in any way that suggests the licensor endorses you or your use.

No additional restrictions

You may not apply legal terms or technological measures that legally restrict others from doing anything the license permits.

***Cogent Engineering* (ISSN: 2331-1916) is published by Cogent OA, part of Taylor & Francis Group.**

Publishing with Cogent OA ensures:

- Immediate, universal access to your article on publication
- High visibility and discoverability via the Cogent OA website as well as Taylor & Francis Online
- Download and citation statistics for your article
- Rapid online publication
- Input from, and dialog with, expert editors and editorial boards
- Retention of full copyright of your article
- Guaranteed legacy preservation of your article
- Discounts and waivers for authors in developing regions

Submit your manuscript to a Cogent OA journal at www.CogentOA.com

